Article

Synthesis of peptoid-based class I selective histone deacetylase inhibitors with chemosensitizing properties

Viktoria Krieger, Alexandra Hamacher, Fangyuan Cao, Katharina Stenzel, Christoph G. W. Gertzen, Linda Schäker-Hübner, Thomas Kurz, Holger Gohlke, Frank J. Dekker, Matthias U. Kassack, and Finn K. Hansen

Just Accepted

Synthesis of peptoid-based class I selective histone deacetylase inhibitors with chemosensitizing properties

Viktoria Krieger,[†,#] Alexandra Hamacher,[†,#] Fangyuan Cao,[#] Katharina Stenzel,[†]

Christoph G. W. Gertzen,[†,¶||] Linda Schäker-Hübner,[§] Thomas Kurz,[†] Holger Gohlke,[†,||]

Frank J. Dekker,[#] Matthias U. Kassack,*[†,‡] and Finn K. Hansen*[§,‡]

†Institut für Pharmazeutische und Medizinische Chemie, Heinrich-Heine-Universität

Düsseldorf, Universitätsstr. 1, 40225 Düsseldorf, Germany.

#Department of Chemical and Pharmaceutical Biology, Groningen Research Institute of

Pharmacy, University of Groningen, Antonius Deusinglaan 1, 9713 AV Groningen, The

Netherlands.

[||]John von Neumann Institute for Computing (NIC), Jülich Supercomputing Centre (JSC),

and Institute for Complex Systems - Structural Biochemistry (ICS-6), Forschungszentrum

Jülich GmbH, Wilhelm-Johnen-Straße, 52425 Jülich, Germany.

[¶]Center for Structural Studies (CSS),Heinrich-Heine-Universität Düsseldorf,

Universitätsstr. 1, 40225 Düsseldorf, Germany.

[§]Pharmaceutical/Medicinal Chemistry, Institute of Pharmacy, Medical Faculty, Leipzig

University, Brüderstraße 34, 04103 Leipzig, Germany.

KEYWORDS

Histone deacetylases, HDAC inhibitors, peptoids, cancer, cisplatin

ABSTRACT

There is increasing evidence that histone deacetylase (HDAC) inhibitors can

(re)sensitize cancer cells for chemotherapeutics via 'epigenetic priming'. In this work, we

describe the synthesis of a series of class I selective HDAC inhibitors with 2-

aminoanilides as zinc-binding groups. Several of the synthesized compounds revealed potent inhibition of the class I HDAC isoforms HDAC1, 2, and/or 3 and promising antiproliferative effects in the human ovarian cancer cell line A2780 and the human squamous carcinoma cell line Cal27. Selected compounds were investigated in a cellular model of platinum resistance. In particular compound **2a** revealed potent chemosensitizing properties and full reversal of cisplatin resistance in Cal27CisR cells. This effect is related to a synergistic increase in caspase 3/7 activation and induction of apoptosis. Thus, this work demonstrates that pan-HDAC inhibition or dual class I/class IIb inhibition is not required for full reversal of cisplatin resistance.

INTRODUCTION

Diverse cellular functions are regulated by dynamic modifications, metabolism, transcription, and translation.[1] The acetylation and deacetylation of lysine belongs to crucial post-translational modifications in the epigenetic field. Epigenetics deals with heritable changes in gene expression without influence of the DNA sequence itself.[1] One way to alter gene expression is the histone acetylation status, which is controlled via

histone acetyl transferases (HATs) and histone deacetylases (HDACs). HDAC proteins

are responsible for the deacetylation of lysine residues located on the amino-terminal tails

of histone proteins. The deacetylation induces condensed and transcriptionally inactive

heterochromatin. Interference with the acetylation/deacetylation process has been linked

to cancer development. Inhibition of HDACs, which are overexpressed in several cancer

types, results in the expression of genes leading to terminal differentiation, growth arrest

and/or apoptosis in cancer cells.[2] Thus, the inhibition of HDACs has become an important

target in cancer research. To date, four HDAC inhibitors (HDACi) have received FDA-

approval in cancer treatment. The first three approvals for HDACi (vorinostat, romidepsin,

and belinostat; Figure 1) have been granted for the treatment of rare types of lymphoma

(cutaneous T-cell lymphoma (CTCL) and/or peripheral T-cell lymphoma (PTCL)).

However, the approval of panobinostat (Figure 1) to treat multiple myeloma is a good

evidence for the application of HDACi in more common cancer types.[3] Beyond

hematologic cancers, HDACi have reached advanced stages of clinical studies in solid

cancers.[3] Furthermore, HDACi have shown therapeutic potential in several other

diseases beyond cancer such as parasitic diseases, immune disorders, HIV, inflammation, and neurodegenerative diseases.[4]

In humans, 18 different HDAC isoforms have been described and classified into four classes based on their homology to yeast HDACs. Class I (HDAC1, 2, 3, 8), class IIa (HDAC4, 5, 7, 9), class IIb (HDAC6, 10), and class IV (HDAC11) HDACs are Zn^{2+}-dependent enzymes, whereas class III HDACs are NAD^+-dependent (sirtuins).[5] The aforementioned hydroxamate-based HDACi (vorinostat, belinostat, and panobinostat) do not exert selectivity towards a specific isoform. In addition, the potential genotoxicity of hydroxamate-containing HDACi represents a major drawback in their application and has fueled the search for alternative ZBGs.[6] In this regard, 2-aminoanilides have emerged as promising alternatives to hydroxamates. Notably, they possess a different isoform profile compared to most hydroxamates and do not exhibit genotoxicity.[3,6] In detail, 2-aminoanilides display selectivity for HDAC1, HDAC2, and HDAC3, which can be further fine-tuned towards HDAC1 and HDAC2 by the introduction of bulky (hetero)aromatic substituents in the 5-position of the 2-aminoanilide scaffold. In the latter case, the

additional (hetero)aromatic group is binding to a hydrophobic 14 Å cavity (the so-called

"foot pocket")[7] in HDAC1 and HDAC2.

There is increasing evidence that 2-aminoanilides can succeed in clinical trials. For

instance, chidamide (tucidinostat, Figure 1B) has been approved in China for relapsed or

refractory PTCL.[8] Furthermore, entinostat (MS-275, Phase III, Figure 1B), mocetinostat

(MGCD0103, Phase II, Figure 1B), and RG2833 (RGFP109, Phase I, Figure 1B) show

selective inhibition of class I HDACs and are currently studied in different stages of clinical

trials.[3,9] Interestingly, RG2833 is developed as drug against the neurodegenerative

disease Friedreich ataxia (FRDA), which highlights the therapeutic potential of

aminoanilide-based HDACi beyond oncology.[9]
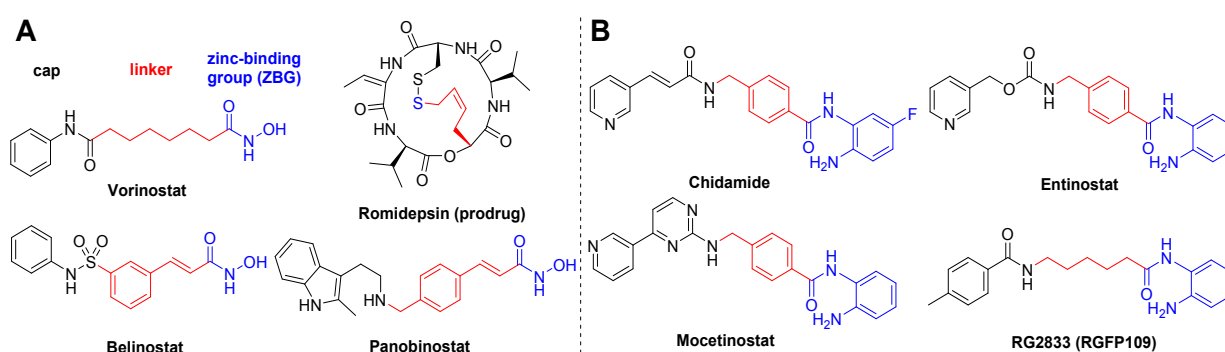
Figure 1. FDA approved HDACi (A) and aminoanilide-based HDACi (B).

We previously discovered hydroxamate-based HDACi utilizing peptoid-based cap groups, which are accessible by a facile synthetic protocol based on the Ugi four-component reaction (U-4CR).[10,11] Peptoid-based hydroxamates with a benzyl linker were identified as HDAC6 preferential inhibitors,[10] whereas hydroxamic acids with an alkyl linker displayed a preference for class I isoforms.[11] Several peptoid-based hydroxamates showed promising chemosensitizing properties and were able to revert cisplatin resistance in cancer cells.[10,11] Due to the aforementioned drawbacks of hydroxamic acids, we aimed at the development of peptoid-based HDACi with a 2-aminoanilide ZBG. We herein report on the rational design, diversity-oriented synthesis, and biological evaluation of class I selective HDACi with peptoid-based cap groups.

RESULTS AND DISCUSSION

Design and Synthesis of Peptoid-Based 2-Aminoanilides.
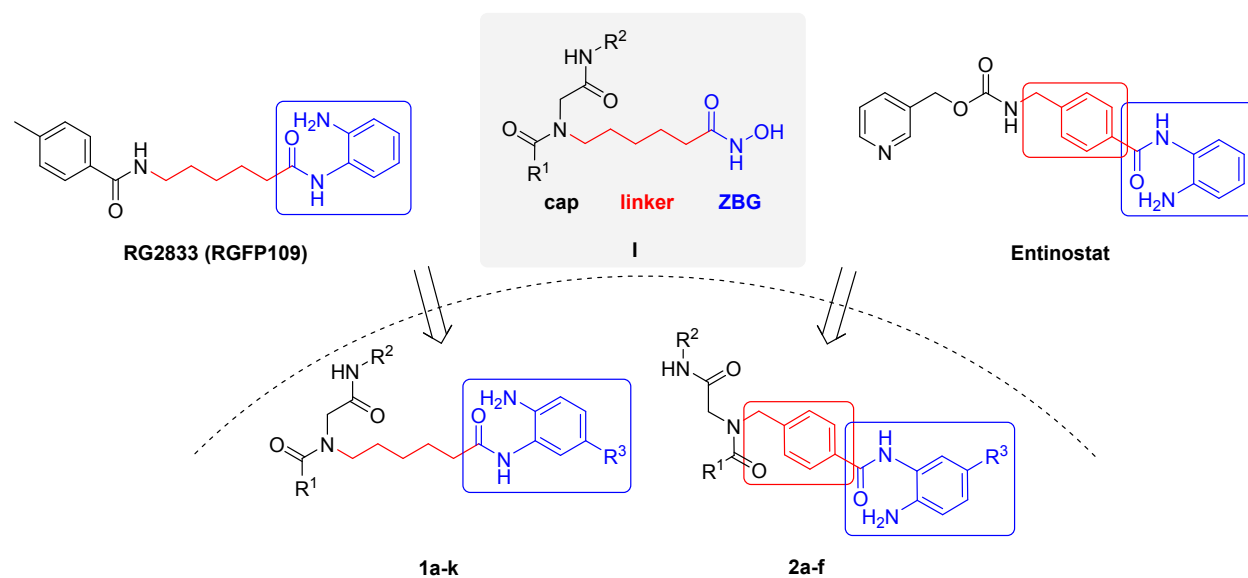
Figure 2. Design of target compounds **1a-k** and **2a-f**.

The synthesis of our HDACi library is summarized in Schemes 1-3. The series of HDACi

1a-k was designed as hybrid compounds derived from our peptoid-based hydroxamate

scaffold **I** and **RG2833** (Figure 2). We retained the aliphatic linker and substituted the

hydroxamate-based ZBG by an aminoanilide-based ZBG in order to improve the

selectivity for the class I isoforms HDAC1-3. The synthesis of the compounds **1a-h** was

achieved through straightforward U-4CRs differing in the use of the carboxylic acid and

the isocyanide components (Scheme 1). In detail, for the synthesis of compounds **3a-h**

the amine methyl 6-aminohexanoate hydrochloride, trimethylamine, and

paraformaldehyde were stirred in dry methanol in the presence of 4 Å molecular sieves

(4 Å MS) to provide the imine intermediate. The subsequent addition of the carboxylic

acid and isocyanide component provided the desired Ugi products **3a-h** after purification

by flash column chromatography (Scheme 1).

Scheme 1. Synthesis of benzamide HDACi **1a-h**.[a]
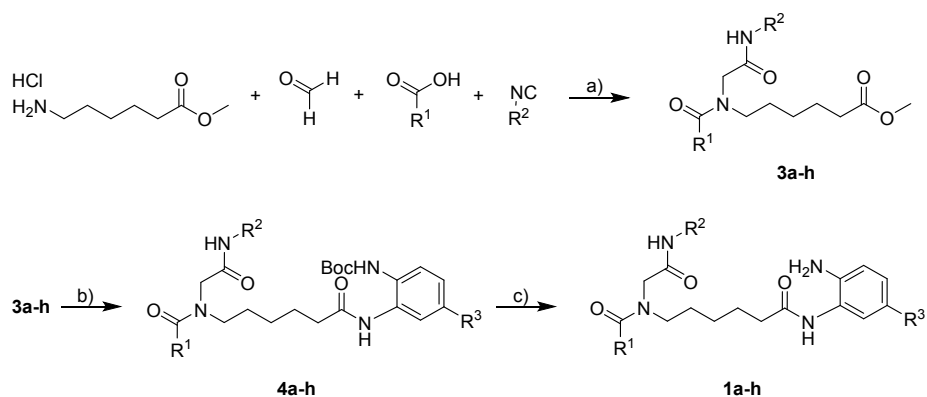
[a]Reagents and conditions: a) (i) Methyl 6-aminohexanoate hydrochloride (1.2 eq),

paraformaldehyde (1.2 eq), MeOH, 4 Å MS, RT, 30 min; (ii) R^1COOH (1 eq), RT, 10 min;

(iii) R^2NC (1 eq), RT, 16h; b) (i) LiOH·H_2O (2 eq), MeOH, RT, 16h; (ii) acid (1.2 eq), amine

(1 eq), pyridine (2 eq), DIC (1.2 eq), HOAt (1.2 eq), CH_2Cl_2/DMF (1:1, v/v), RT, 16h; c)

TFA/CH_2Cl_2 (1:5, v/v), RT, 30 min.

The target compounds **1a-h** were subsequently prepared by performing suitable post-Ugi

transformations. The methyl esters of **3a-h** were cleaved via hydrolysis with LiOH·H_2O in

methanol overnight. Afterwards, the resulting carboxylic acids were coupled with the

respective mono-Boc-protected phenylenediamine derivative using the coupling reagents

DIC and HOAt in the presence of pyridine in CH_2Cl_2/DMF to afford the Boc-protected

compounds **4a-h**. Finally, the acidic deprotection yielded the desired peptoid-based

HDACi **1a-h**.

Scheme 2. Submonomer synthesis of compound **1i**.[a]
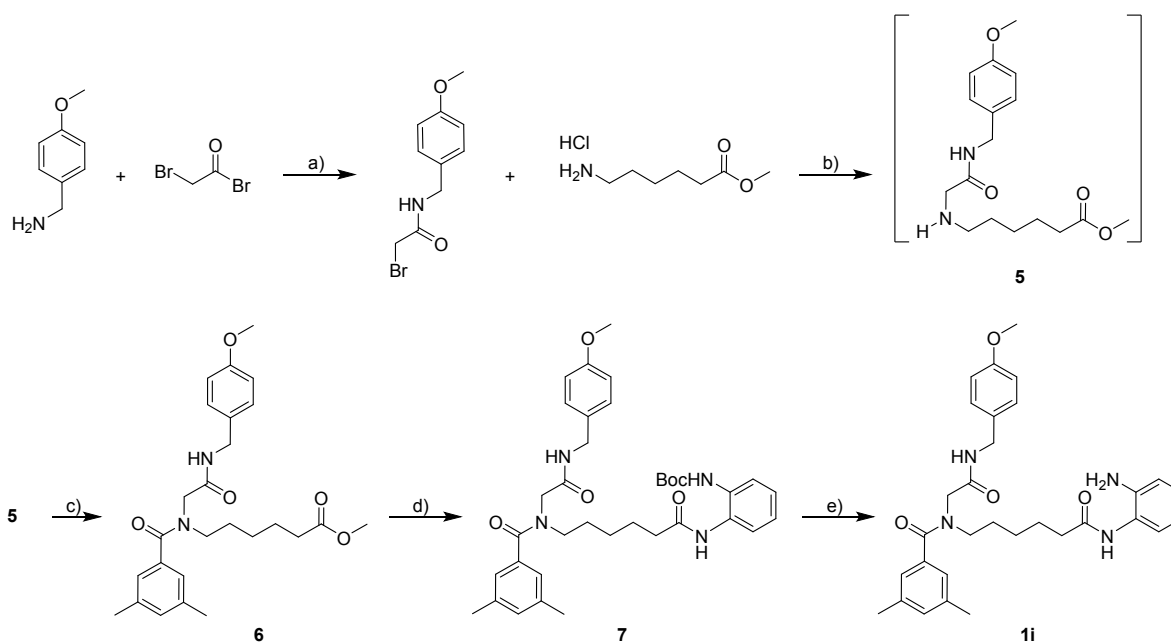
^aReagents and conditions: a) (4-Methoxyphenyl)methanamine (1 eq), 2-bromoacetyl bromide (1 eq), DIPEA (1 eq), CH$_2$Cl$_2$, 0 °C→RT, 16 h; b) methyl 6-aminohexanoate hydrochloride (1 eq), 2-bromo-*N*-(4-methoxybenzyl)acetamide (1 eq), Et$_3$N (2 eq), CH$_2$Cl$_2$, RT, 16 h; c) methyl 6-({2-[(4-methoxybenzyl)amino]-2-oxoethyl}amino)hexanoate (1.2 eq), pyridine (1.2 eq), 3,5-dimethylbenzoyl chloride (1 eq), CH$_2$Cl$_2$, 0 °C→RT, 16 h; d) (i) LiOH·H$_2$O (2 eq), MeOH, RT, 16 h; (ii) acid (1.2 eq), *tert*-butyl (2-aminophenyl)carbamate (1 eq), pyridine (2 eq), DIC (1.2 eq), HOAt (1.2 eq), CH$_2$Cl$_2$/DMF (1:1, v/v), RT, 24 h; e) TFA/CH$_2$Cl$_2$ (15%, v/v), RT, 30 min.

Scheme 3. Submonomer synthesis of compounds **1j,k**.[a]

8

9

10a,b

11a,b

1j,k
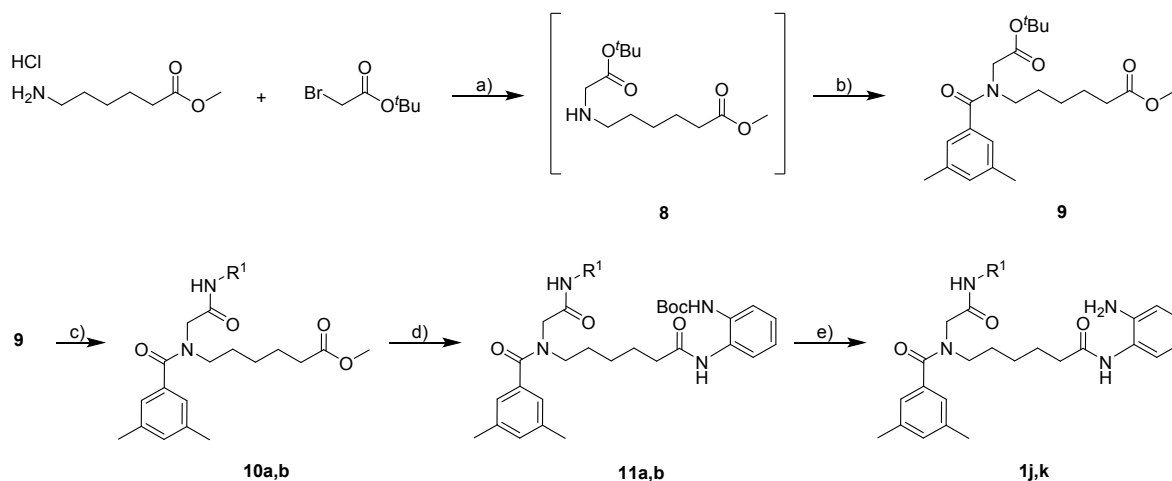
[a]Reagents and conditions: a) Methyl 6-aminohexanoate hydrochloride (1 eq), *tert*-butyl

bromoacetate (1 eq), Et$_3$N (2 eq), THF, RT, 16 h; b) methyl 6-{[2-(*tert*-butoxy)-2-oxoethyl]-

amino}hexanoate (1.2 eq), pyridine (1.2 eq), 3,5-dimethylbenzoyl chloride (1 eq), CH$_2$Cl$_2$,

RT, 18 h; c) (i) TFA/CH$_2$Cl$_2$ (1:5, v/v), RT, 2 h; (ii) acid (1 eq), amine (1 eq), EDC·HCl (2

eq), DMAP (0.4 eq), DMF/CH$_2$Cl$_2$, RT, 16 h; d) (i) LiOH·H$_2$O (2 eq), MeOH, RT, 16 h; (ii)

acid (1.2 eq), *tert*-butyl (2-aminophenyl)carbamate (1 eq), pyridine (2 eq), DIC (1.2 eq),

HOAt (1.2 eq), CH$_2$Cl$_2$/DMF (1:1, v/v), RT, 24 h; e) TFA/CH$_2$Cl$_2$ (15%, v/v), RT, 30 min.

Since the number of purchasable isocyanides is limited, we switched to a peptoid

submonomer synthesis for further modifications of the isocyanide region (Scheme 2 and

3). The synthesis of compound **1i** is illustrated in Scheme 2. The reaction of 4-

methoxybenzylamine with bromoacetyl bromide in the presence of DIPEA afforded the

corresponding bromoacetyl amide. The subsequent alkylation of methyl 6-

aminohexanoate hydrochloride in the presence of triethylamine in dichloromethane

yielded the secondary amine **5**. Intermediate **5** was directly treated with 3,5-

dimethylbenzoyl chloride using pyridine as a base to generate the peptoid **6**. The methyl

ester in **6** was hydrolyzed and the resulting carboxylic acid derivative was subjected to an

amide coupling reaction with mono-Boc-protected phenylenediamine to yield **7**. Removal

of the Boc-protecting group furnished the desired aminoanilide **1i**.

The synthesis of the HDACi **1j,k** was performed as highlighted in Scheme 3. The

alkylation of methyl 6-aminohexanoate hydrochloride with *tert*-butyl bromoacetate in the

presence of triethylamine in THF provided the secondary amine **8**. Without further

purification, the intermediate **8** was directly acylated with 3,5-dimethylbenzoyl chloride

using pyridine as a base to furnish the key building block **9**. Subsequently, **9** was used as

starting point for the variation of the isocyanide region. To this end, we performed the

deprotection of the *tert*-butyl group followed by amide coupling reactions of the free

carboxylic acid with the respective amine using DIC and HOAt as coupling agents to

furnish **10a,b**. The HDACi **1j,k** were prepared via the saponification of the methyl ester in

10a,b and a subsequent amide coupling with *tert*-butyl (2-aminophenyl)carbamate to yield

11a,b. Next, the Boc-protecting group was removed by acidolysis to afford the target

compounds **1j,k**.

The second type of HDACi **2a-f** (Figure 2) is derived from our peptoid-based hydroxamate

scaffold **I** and entinostat (MS-275), a selective inhibitor of HDAC1, HDAC2, and HDAC3.

Compared to the first type of HDACi **1a-k** they differ in their linker. The synthesis of

compounds **2a-f** was performed essentially as described for compounds **1a-h** (Scheme

4). Briefly, in the case of compounds **2a-f** we used methyl 4-(aminomethyl)benzoate as

amine component in the U-4CR to provide the intermediates **12a-f** bearing a benzyl linker.

The Boc-protected aminoanilides **13a-f** were then prepared by hydrolysis of the methyl

ester followed by amide coupling reactions with the respective mono-Boc-protected

phenylenediamine derivative. Finally, deprotection of the Boc group was achieved by

treatment of **13a-f** with trifluoroacetic acid in dichloromethane to provide the peptoid-

based HDACi **2a-f**.

Scheme 4. Synthesis of HDACi **2a-f**.[a]
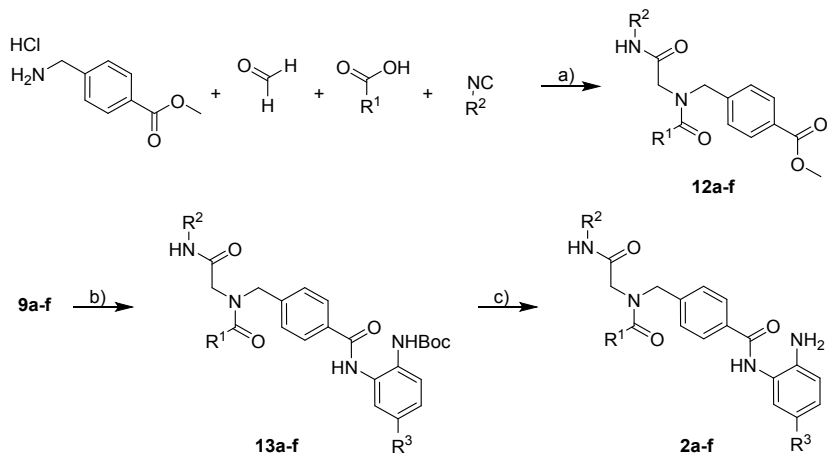
[a]Reagents and conditions: a) (i) Methyl 4-(aminomethyl)benzoate hydrochloride (1.2 eq),

paraformaldehyde (1.2 eq), MeOH, 4 Å MS, RT, 30 min; (ii) R^1COOH (1 eq), RT, 10 min;

(iii) R^2NC (1 eq), RT, 16h; b) (i) LiOH·H_2O (2 eq), MeOH, RT, 16h; (ii) acid (1.2 eq), amine

(1 eq), EDC·HCl (2 eq), DMAP (0.4 eq), RT, 16h; c) TFA/CH_2Cl_2 (1:5, v/v), RT, 30 min.
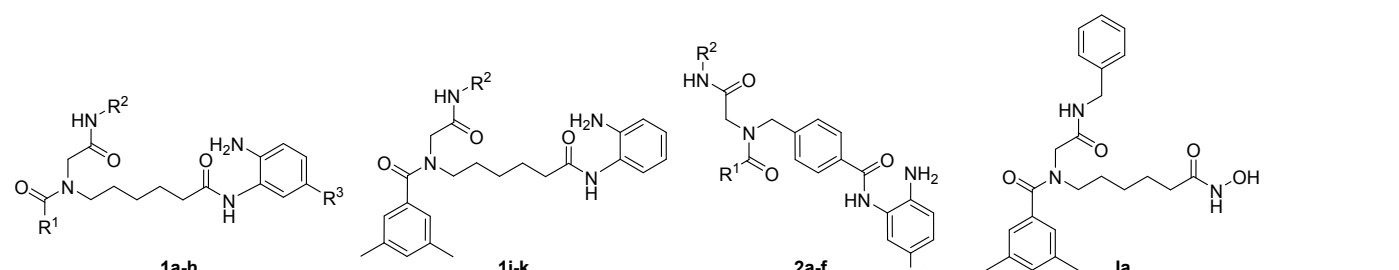
Inhibition of HDAC1-3 and HDAC6. All synthesized compounds and the reference HDACi

vorinostat were first screened for inhibitory activity against their intended targets HDAC1-

3. Furthermore, HDAC6 was selected as control isoform. The results are summarized in

Table 1. As expected, all aminoanilides were inactive against HDAC6 (IC_{50} > 10 µM). The

screening against HDAC1-3 provided some interesting differences depending on the type

of the linker and ZBG. In general, the 2-aminoanilides with a benzyl linker exhibited

increased activity against HDAC1 and HDAC2 compared to their corresponding alkyl

linker counterparts, whereas the alkyl-based compounds showed higher activity against

HDAC3 (see e.g. **1c** vs **2a**). Compound **1h** bearing a phenyl ring in R^3 position, which is

intended to target the foot pocket in HDAC1 and HDAC2, represents one noteworthy

exemption. **1h** revealed clearly the highest activity against HDAC1 (IC_{50}: 0.057 µM)

among the alkyl-based compounds and is almost inactive against HDAC3 (20% inhibition

at 10 µM). Interestingly, compound **1d** utilizes the same cap and linker as compound **1h**

and the only difference in the structure is the additional phenyl ring at the R^3 position. The

introduction of this foot pocket targeting moiety leads to an ~20-fold improved potency of

1h towards HDAC1 and a >40-fold reduction in activity against HDAC3 compared to **1d**.

The hydroxamic acid-based HDACi **Ia** (Table 1), one of the hit compounds from our previous study,[11] represents the corresponding hydroxamate analogue of **1d** and **1h**. This compound showed potent inhibition of HDAC1-3 and 6 with IC_{50} values ranging from 0.025 to 0.135 µM. Interestingly, the HDAC selectivity profile of this compound can be altered towards HDAC3 preferential inhibition by replacing the hydroxamate with an unsubstituted aminoanilide or towards HDAC1 preferential inhibition via the introduction of a foot pocket targeting moiety.

In the case of the benzyl-based compounds, no noteworthy change in potency against HDAC1 was observed after introduction of an additional phenyl ring at the aminoanilide group (see **2a** (IC_{50}: 0.038 µM) vs **2e** (IC_{50}: 0.039 µM)). As expected, compound **2e** was inactive against HDAC3. Notably, the introduction of a fluorine atom in R^3 position, as realized in the approved aminoanilide chidamide, resulted in a significant decrease of the HDAC1 and 2 inhibition (see **2b** vs **2f**) and hence this substitution appears to be detrimental for our peptoid-based aminoanilides. Compared to the well-known aminoanilide entinostat (HDAC1 IC_{50}: 0.519 µM, HDAC2 IC_{50}: 0.505 µM, and HDAC3

IC$_{50}$: 2.85 µM,), our benzyl-based compounds **2a-f** displayed an improved inhibition of

HDAC1 and a clear preference for HDAC1 over HDAC2 and 3 (Table 1).

Table 1. Inhibitory activities (IC$_{50}$ [µM]) of compounds **1a-k** and **2a-f** against HDACs 1-3,

and 6.

compd	R^1	R^2	R^3	IC$_{50}$ [µM]			
				HDAC1	HDAC2	HDAC3	HDAC6
1a	Ph	c-Hex	H	5.46±0.32	5.95±0.67	0.858±0.066	>10[b]
1b	3,5-Me-Ph	c-Hex	H	5.55±0.30	6.66±0.44	0.481±0.088	>10[b]
1c	4-Me$_2$N-Ph	Bn	H	1.58±0.15	1.24±0.078	0.312±0.021	>10[b]
1d	3,5-Me-Ph	Bn	H	1.16±0.21	1.60±0.38	0.250±0.021	>10[b]
1e	1-Naphthyl	c-Hex	H	6.56±0.84	5.38±0.69	0.646±0.066	>10[b]
1f	1-Naphthyl	Bn	H	1.67±0.17	1.90±0.030	0.163±0.013	>10[b]
1g	4-Me$_2$N-Ph	Bn	F	1.98±0.028	3.06±0.16	0.369±0.009	>10[b]
1h	3,5-Me-Ph	Bn	Ph	0.057±0.005	1.81±0.12	20% @ 10 µM[a]	>10[b]
1i	3,5-Me-Ph	4-MeO-Bn	H	2.08±0.21	30% @ 10 µM[a]	49% @ 10 µM[a]	>10[b]
1j	3,5-Me-Ph	4-Me-Bn	H	1.10±0.05	5.03±0.69	0.478±0.026	>10[b]
1k	3,5-Me-Ph	3,5-Me-Bn	H	0.484±0.051	4.10±0.29	0.583±0.027	>10[b]
2a	4-Me$_2$N-Ph	Bn	H	0.038±0.012	0.283±0.028	0.586±0.055	>10[b]

2b	3,5-Me-Ph	Bn	H	0.062±0.012	0.485±0.018	32% @ 10 µM[a]	>10[b]
2c	3-Pyridyl	Bn	H	0.103±0.016	0.786±0.017	0.878±0.117	>10[b]
2d	3,5-Me-Ph	Bn	Ph	0.051±0.011	34% @ 3.33 µM[a]	>10000[b]	>10[b]
2e	4-Me$_2$N-Ph	Bn	Ph	0.039±0.011	36% @ 3.33 µM[a]	>10000[b]	>10[b]
2f	3,5-Me-Ph	Bn	F	0.277±0.045	25% @ 10 µM[a]	23% @ 10 µM[a]	>10[b]
vorinostat	---	---	---	0.111±0.015	0.146±0.014	0.0097±0.0008	0.102±0.009
entinostat	---	---	---	0.519±0.063	0.505±0.028	2.85±0.22	>10[b]
RG2833	---	---	---	$K_i = 0.032$[c]	n.d.	$K_i = 0.005$[c]	n.d.
1a	3,5-Me-Ph	Bn	---	0.025±0.007[d]	0.061±0.003[d]	0.026±0.002[d]	0.135±0.013[d]

[a]% inhibition at the concentration stated (µM). [b]<15% inhibition at 10 µM. [c]data taken from

9b. [d]data taken from ref. 11.

Interestingly, compounds **1h** (alkyl linker) and **2d** (benzyl linker) bearing the same cap

and ZBG revealed similar inhibition profiles with potent inhibition of HDAC1 (**1h** (IC_{50}:

0.057 µM) vs **2d** (IC_{50}: 0.051 µM)) and weak inhibition of HDAC2 and 3. In contrast,

compounds **1c** and **2a**, which also only differ in the linker, showed a completely different

inhibition profile with **1c** being an HDAC3 preferential inhibitor, whereas **2a** displayed

HDAC1 preference. Based on these results, it can be assumed that, in the absence of a

foot pocket group, the linker dictates the selectivity profile. However, as soon as a foot

pocket targeting moiety is added to the aminoanilide ZBG, the ability of the substituted

aminoanilide ZBG to occupy the foot pocket is responsible for the preferential inhibition

of HDAC1.

The most important structure–activity and structure–selectivity relationships are

summarized in Figure 3. Overall, this screening revealed the alkyl-based compound **1f** as

the most potent preferential HDAC3 inhibitor and the benzyl-based compounds **2d,e** as

preferential HDAC1 inhibitors. Furthermore, **1h** and **2a** were identified as the most potent

HDAC1 inhibitors from the alkyl and benzyl series, respectively.

Cap-effects:
- Strongest HDAC1 inhibition in the alkyl series (**1h**): R^1 = 3,5-Me-Ph, R^2 = 3,5-Me-Bn; R^3 = Ph.

- Strongest HDAC1 inhibition in the benzyl series (**2a**): R^1 = 4-Me$_2$N-Ph, R^2 = Bn; R^3 = H.

Benzyl linker:
- increases HDAC1 and 2 inhibition

Pentyl linker:
- enchances HDAC3 inhibition and selectivity

Fluorine substitution:
- decreased HDAC inhibition

Phenyl substituent:
- improves HDAC1 inhibition in combination with a pentyl linker

Phenyl substituent:
- improves HDAC1 selectivity in combination with a benzyl linker

Figure 3. Structure-activity and structure-selectivity relationships of the peptoid-based aminoanilides **1a-k** and **2a-f**.

Docking Studies. Compounds **1h** and **2a**, which showed the highest activity against HDAC1 within each molecule series, respectively, and **1f**, which showed preferential inhibition of HDAC3, were docked into energetically relaxed X-ray crystal structures of HDAC1, HDAC2, HDAC3, and HDAC6. We docked the three compounds in both their *cis*- and *trans*-rotamers, considering the orientation of the amide bond connecting R^1. While valid docking poses of all three compounds were identified in HDAC1 and HDAC2, molecular docking failed in the case of HDAC6: Here, no docking pose could be identified in which the ZBG of the respective compound was interacting with the Zn^{2+} ion at the catalytic center of HDAC6 (Table S1). The reason for this is the shape of the catalytic center in HDAC6, which is too narrow to accommodate the sterically demanding ZBG of the compounds. As the interaction of the ZBG with the zinc ion is known to be essential for the activity of HDACi, these results are in perfect agreement with the compounds' inability to inhibit HDAC6 (Table 1). Both **1f** and **2a** furthermore produce valid docking

poses in HDAC3 (Table 1). Thus, the docking results neither replicate the HDAC3

preference of **1f** nor the HDAC1 preference of **2a**; however, given the small differences

in the respective IC_{50} values (Table 1), such a discrimination cannot be expected from a

scoring function.[12] Yet, the docking results do reflect the compounds' general ability to

inhibit the three HDAC isoforms (Table 1). The validity of the docking is further

corroborated by the results of compound **1h**, for which valid docking poses were obtained

in HDAC1 and HDAC2, but not in HDAC3 (Table S1), in line with inhibition studies (Table

1).

Judging from the docking results of the three HDACi, the binding affinity to HDAC1 seems

to be dominated by the aromatic character and size of the ZBG and linker. As such, **1h**

and **2a**, which show a high affinity towards HDAC1, bear an additional phenyl ring in their

structure: In **1h**, the phenyl ring is in position R^3, with which it occupies the foot pocket

adjacent to the zinc ion of HDAC1 (Figure 4A); in **2a**, the phenyl ring is in the linker forming

π-stacking interactions to H178 (Figure 4B). In contrast, **1f**, which shows a lower affinity

towards HDAC1 than the other two compounds, bears neither of the two aforementioned

features. For the substituents in R^1 and R^2, no common interaction pattern can be found for all three tested HDACi. While **1f** and **1h** both interact with Y204, **1h** forms hydrophobic contacts to L271, and **1f** forms π-stacking interactions with H28 (Figure 4A+C). H28 is also addressed by π-stacking interactions by **2a**, yet R^1 of this compound forms π-stacking interactions with F205. The inability of **1h** to inhibit HDAC3 is caused by a spacious phenyl ring in R^3, which does not fit the binding pocket of HDAC3. As the residues lining the binding pocket of HDAC1 and HDAC2 are highly identical (96%, considering residues 8 Å around the co-crystallized ligand of the HDAC2 complex structure as part of the binding pocket), similar docking results for both isoforms could be expected. However, the energetic relaxation of the two structures widened the brim of the HDAC2 binding pocket by ~1 Å more than that of HDAC1, which allows HDAC2 to also accommodate the more spacious *trans*-rotamers of the HDACi.

To conclude, while the docking cannot reproduce subtle selectivity differences, it is able to correctly predict and rationalize the ligands' general capabilities to inhibit the HDAC isoforms 1, 2, and 3.
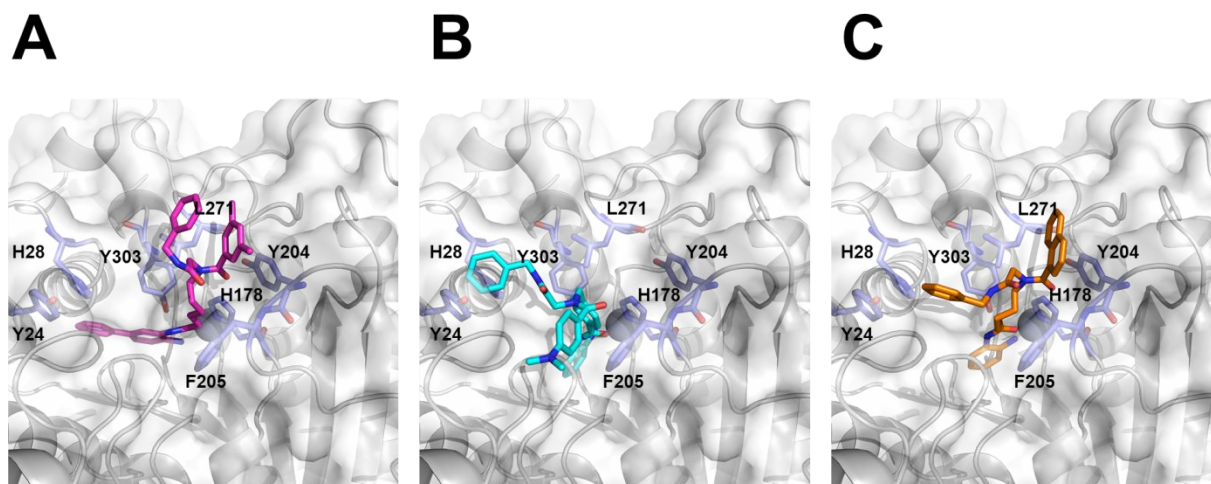
Figure 4. Predicted binding modes of compounds *cis*-**1h** (**A**, magenta), *cis*-**2a** (**B**, light

blue), and *cis*-**1f** (**C**, orange) in the energetically relaxed X-ray crystal structure of HDAC1

(white, cartoon and surface, PDB ID 4BKX). Prominent interacting residues of HDAC1

are shown in navy sticks. **A** Compound *cis*-**1h** utilizes its spacious ZBG to fill the

hydrophobic foot pocket in HDAC1 and engages in π-stacking interactions with Y204. **B**

Compound *cis*-**2a** engages in π-stacking interactions with H28 and F205. **C** Compound

cis-**1f** engages in π-stacking interactions with H28 and Y204.

Anticancer Activity and Inhibition of Cellular HDAC Activity. All aminoanilide HDACi **1a-k**

and **2a-f** were assessed for their cytotoxicity and HDAC inhibitory activity in the human

ovarian cancer cell line A2780 and the human tongue squamous cell carcinoma cell line
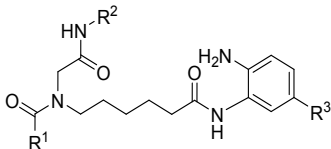
Cal27. Results are summarized in Tables 2 and 3.

Table 2. Cytotoxic activity of compounds **1a-k** and **2a-f**.[a]
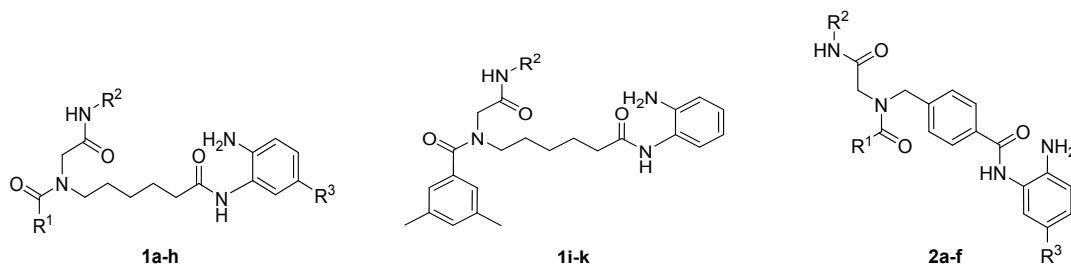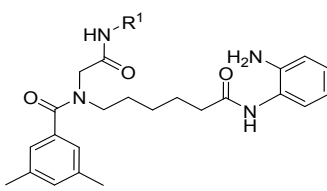
compd	R^1	R^2	R^3	MTT IC$_{50}$ [µM]	
				A2780	Cal27
1a	Ph	c-Hex	H	181	30.9
1b	3,5-Me-Ph	c-Hex	H	42.0	17.5
1c	4-Me$_2$N-Ph	Bn	H	18.5	16.0
1d	3,5-Me-Ph	Bn	H	20.9	13.7
1e	1-Naphthyl	c-Hex	H	18.1	24.9
1f	1-Naphthyl	Bn	H	22.8	11.0
1g	4-Me$_2$N-Ph	Bn	F	25.9	20.2
1h	3,5-Me-Ph	Bn	Ph	17.1	18.9
1i	3,5-Me-Ph	4-MeO-Bn	H	24.6	17.4
1j	3,5-Me-Ph	4-Me-Bn	H	9.80	18.2
1k	3,5-Me-Ph	3,5-Me-Bn	H	5.10	19.3
2a	4-Me$_2$N-Ph	Bn	H	2.40	1.60
2b	3,5-Me-Ph	Bn	H	2.80	1.60
2c	3-Pyridyl	Bn	H	8.90	11.2
2d	3,5-Me-Ph	Bn	Ph	n.e.	8.90
2e	4-Me$_2$N-Ph	Bn	Ph	n.e.	11.1
2f	3,5-Me-Ph	Bn	F	5.40	5.72
vorinostat	---	---	---	2.42	2.64
cisplatin	---	---	---	2.25	2.50

1
2
3
4
5
6
7
8
9
10
11
12
13
14
15
16
17
18
19
20
21
22
23
24
25
26
27
28
29
30
31
32
33
34
35
36
37
38
39
40
41
42
43
44
45
46
47
48
49
50
51
52
53
54
55
56
57
58
59
60

^{a}Values are the mean of three experiments. Standard deviations are <10% of the mean. n.e. = no effect up to 100 µM.

Table 3. HDAC inhibition of compounds **1a-k** and **2a-f**.^{a}

1a-h   1i-k   2a-f

compd	R^1	R^2	R^3	HDACi IC$_{50}$ [µM]	
				A2780	Cal27
1a	Ph	c-Hex	H	43.6	21.9
1b	3,5-Me-Ph	c-Hex	H	22.8	12.1
1c	4-Me$_2$N-Ph	Bn	H	9.25	4.33
1d	3,5-Me-Ph	Bn	H	8.71	3.93

1e	1-Naphthyl	c-Hex	H	33.1	13.0
1f	1-Naphthyl	Bn	H	10.2	4.13
1g	4-Me$_2$N-Ph	Bn	F	13.4	6.82
1h	3,5-Me-Ph	Bn	Ph	1.43	0.47
1i	3,5-Me-Ph	4-MeO-Bn	H	3.53	4.81
1j	3,5-Me-Ph	4-Me-Bn	H	4.48	4.57
1k	3,5-Me-Ph	3,5-Me-Bn	H	3.17	3.15
2a	4-Me$_2$N-Ph	Bn	H	0.48	0.11
2b	3,5-Me-Ph	Bn	H	0.81	0.18
2c	3-Pyridyl	Bn	H	1.06	1.01
2d	3,5-Me-Ph	Bn	Ph	1.72	0.63
2e	4-Me$_2$N-Ph	Bn	Ph	2.62	0.85
2f	3,5-Me-Ph	Bn	F	1.43	0.47
vorinostat	---	---	---	0.96	0.86

[a]Values are the mean of three experiments. Standard deviations

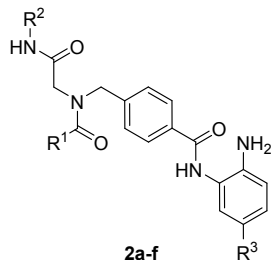are <10% of the mean. n.e. = no effect up to 100 µM.

The compounds revealed cytotoxic activity with IC$_{50}$ values in the range of 1.60 µM up to

181 µM (and two compounds, **2d** and **2e**, with no effect up to 100 µM) depending on their

substitution pattern and the cell line investigated. In the whole cell HDAC assay, the

compounds showed HDAC inhibitory activity from lower nM range (0.11 µM) up to 43.6

µM. Overall, data from both assays (pIC$_{50}$ values MTT and cellular HDAC assays) show

significant correlation (A2780: r^2: 0.7236; Cal27: r^2: 0.6816). **2a** and **2b** were the most potent compounds in both MTT and cellular HDAC assays. **2a** and **2b** were nearly equally cytotoxic in the respective cell lines (IC_{50} of 1.60 µM in Cal27 and IC_{50} of 2.40 and 2.80 µM in A2780). In Cal27, **2a** and **2b** were even more potent than the reference pan-HDACi vorinostat in the MTT (1.7fold) and cellular HDAC assay (approx. 5fold). Whereas **2a** and **2b** inhibit HDAC1 and HDAC2 with similar potency (Table 1), only **2a**, but not **2b**, potently inhibits HDAC3. Thus, for potent cytotoxicity (MTT assay), inhibition of HDAC1 and HDAC2 seems to be sufficient in the cellular model used in this study. However, HDAC1 inhibition only (no HDAC2 inhibition) reduces cytotoxic potency significantly, as can be seen by comparison of **2b** (HDAC1 and HDAC2 inhibitor) with **2d** or **2e** (both selective HDAC1 inhibitors): in MTT assays at Cal27 cells, **2b** has an IC_{50} of 1.6 µM whereas **2d** and **2e** show IC_{50} values of 8.90 and 11.1 µM, respectively. These findings are in agreement with literature reports on redundant functions of HDAC1 and HDAC2 in gene ablation experiments: combined ablation of HDAC1 and HDAC2 resulted in severe proliferation defects.[13] However, in other cancer cells, knockdown of HDAC3 led to growth inhibition and apoptosis.[20] Thus, even though our results suggest a major role for HDAC1

and HDAC2 (and not HDAC3) in Cal27 and A2780 cells, an important contribution of

HDAC3 inhibition cannot be ruled out for other cancer types.

Selection of hit compounds and extended HDAC isoform profile of 1h, 2a, and 2d. Based

on high inhibitory activity against HDAC1 in the enzyme assay (Table 1) and on different

selectivity profiles, we chose compounds **1h** (HDAC1 selective inhibitor with mediocre

HDAC2 and MTT activity), **2a** (most potent compound against HDAC1 and HDAC2 as

well as highest activity in the cellular HDAC and MTT assay), and **2d** (HDAC1 selective

inhibitor with low HDAC2, 3 activity and mediocre activity in the MTT assay) for further

analysis. Aminoanilides are typically inactive against class IIa isoforms. To confirm this,

1h, **2a**, and **2d** were screened for activity against the representative class IIa isoform

HDAC4. Furthermore, all three compounds were tested for their inhibition of the remaining

class I isoform HDAC8. As expected **1h**, **2a**, and **2d** displayed only very weak inhibitory

activity against HDAC4 and HDAC8 (Table 4). The inhibition data of **1h**, **2a**, and **2d**

against HDACs1-4, HDAC6, and HDAC8 are summarized in Table 4. Taken together, the

HDAC isoform profiling discloses compounds **1h** and **2d** as HDAC1 preferential inhibitors

and compound **2a** as a potent HDAC1 inhibitor with weaker, but submicromolar inhibitory

activity against HDAC2 and HDAC3.

Table 4. Inhibitory activities (IC$_{50}$ [µM]) of compounds **1h, 2a, 2d** and vorinostat against

HDACs1-4, HDAC6, and HDAC8.

compd	IC$_{50}$ [µM]					
	HDAC1	HDAC2	HDAC3	HDAC4	HDAC6	HDAC8
1h	0.057±0.005	1.81±0.12	20% @ 10µM[a]	>10	>10	>10
2a	0.038±0.012	0.283±0.028	0.586±0.055	>10	>10	9.21±0.62
2d	0.051±0.011	34% @ 3.33 µM[a]	14% @ 10µM[a]	>10	>10	3.13±0.21
vorinostat	0.111±0.015	0.146±0.014	0.0097±0.0008	42.2±1.2	0.102±0.009	11.9±0.89

[a]% inhibition at the concentration stated (µM).

Enhancement of Cisplatin-Induced Cytotoxicity. The expression of HDACs is

dysregulated in many types of cancer and contributes to the development of drug

resistance.[14] Therefore, the combination of chemotherapeutics such as cisplatin with

HDACi could serve as a strategy to overcome chemoresistance. First, we analyzed the effect of the HDACi **1h**, **2a**, or **2d**, respectively, on the cytotoxic potency of cisplatin in cancer cell lines. Cal27 and Cal27CisR were chosen as model system for cisplatin-sensitive and cisplatin-resistant cell lines.[15] Both cell lines were incubated with 5 µM **1h**, 0.5 µM **2a,** or 3.2 µM **2d** 48 h prior to cisplatin administration for another 72 h followed by MTT readout. Concentrations of **1h**, **2a**, and **2d** were chosen according to cytotoxic effects determined in validation experiments (MTT assays, data not shown). IC_{50} values for cisplatin alone and in combination with **1h**, **2a**, or **2h** together with the corresponding shift factors are shown in Table 5.

**Table 5.** IC_{50} values (µM) after treatment of Cal27 and Cal27CisR with cisplatin or in combination with 5 µM **1h**, 0.5 µM **2a**, 3.2 µM **2d**, or 0.5 µM vorinostat, respectively. SF means shift factor and was calculated as the ratio of the IC_{50} of cisplatin alone and the IC_{50} of the corresponding drug combination.

Compound	Cell line			
	Cal27		Cal27CisR	
	IC_{50}	SF	IC_{50}	SF
Cisplatin	9.79*	---	63.2*	---
Cisplatin + **1h** 5.0 µM	1.86	5.26	15.7	4.03
Cisplatin + **2a** 0.5 µM	1.26	7.77	8.42	7.51
Cisplatin + **2d** 3.2 µM	1.86	5.26	12.0	5.27
Cisplatin + **vorinostat** 0.5 µM	1.96	5.00	9.39	6.73

Data shown are the mean of pooled data from at least three experiments each carried

out in triplicates. The standard deviations are < 10% of the mean. All shift factors are

significant (t-test, $p < 0.05$). *IC_{50} value is higher than reported in Table 3 due to different

incubation time here: 48 h preincubation with **1h**, **2a**, or **2d**, followed by addition of

cisplatin and incubation for 72 h.

48 h preincubation with **1h**, **2a**, or **2d** prior to cisplatin showed a significant enhancement

of cisplatin-induced cytotoxicity. In the parental cell line Cal27, a hypersensitization for

cisplatin was achieved with all three compounds. Shift factors of sensitization ranged from

5.26 for **1h** up to 7.77 for **2a** and were even higher than those obtained with the pan

HDACi vorinostat (shift factor 5.00). Observed shift factors in the cisplatin-resistant

subline Cal27CisR were slightly lower than in Cal27 with the exception of vorinostat. **2a**

(most potent compound in MTT, cellular HDAC, and enzyme HDAC assays) gave the

highest shift factors (7.77 in Cal27; 7.51 in Cal27CisR) and was able to completely

reverse cisplatin resistance in Cal27CisR by shifting the cisplatin IC_{50} from 63.2 µM

(without **2a**) to 8.42 µM (presence of 0.5 µM **2a**), which is slightly below the cisplatin IC_{50}

value of the native cell line Cal27. In addition, **2a** is even superior to vorinostat in

resensitization of Cal27CisR towards cisplatin (shift factor **2a**: 7.51; shift factor vorinostat:

6.73). Figure 5 shows the effect of the most potent compound **2a** on the cytotoxic activity

of cisplatin in Cal27CisR cells.
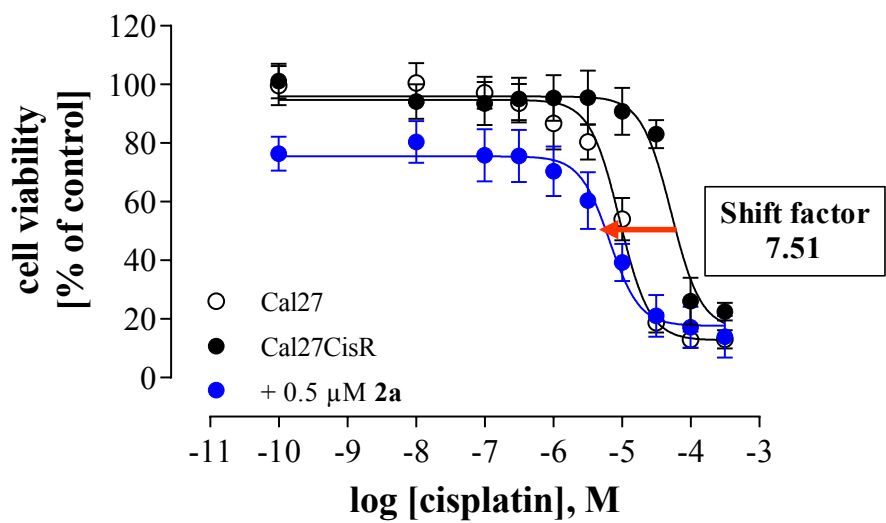
Figure 5. 2a induces complete resensitization of Cal27CisR cells against cisplatin.

Cal27CisR cells were pretreated with 0.5 µM **2a** 48 h prior to application of cisplatin. After

another 72h, IC_{50} values were determined by MTT assay. The shift factor is defined as

the ratio of the IC_{50} of cisplatin alone and the IC_{50} of the corresponding combination with

2a. Data shown are the mean ± SEM of three independent experiments each performed

in triplicates.

To determine the type of interaction between cisplatin and **1h**, **2a**, or **2d**, concentration-

effect analyses were performed. The concentrations used for a 48h preincubation prior to

cisplatin for **1h**, **2a**, and **2d** were the same for Cal27 and Cal27CisR while the cisplatin

concentrations were selected based on the IC_{50} values for each cell line. Table 6 shows

the CI (combination index) values based on the synergy quantification using the Chou-

Talalay method.[16]

Table 6. Interactions between **1h**, **2a**, or **2d**, respectively, and cisplatin. Cal27 and the cisplatin-resistant tumor cell line Cal27CisR were treated with increasing concentrations of cisplatin and **1h**, **2a**, or **2d**. Data shown are CI (combination index) values calculated using CalcuSyn 2.1 software based on the Chou-Talalay method. A CI > 1 indicates antagonism, a CI = 1 indicates an additive effect, and a CI < 1 indicates synergism. CI < 0.2 indicates strong synergism and is marked in bold. * = fraction affected (fa) less than 0.20.

	Cal27				Cal27 CisR		
cisplatin		**1h [μM]**		**cisplatin**		**1h [μM]**	
[μM]	**1.00**	**3.20**	**5.00**	**[μM]**	**1.00**	**3.20**	**5.00**
0.10	*	*	*	**1.00**	*	*	*
0.32	*	*	*	**3.20**	*	*	*
1	*	*	0.76	**10**	*	*	**0.10**
3.2	*	0.25	**0.10**	**32**	*	0.74	**0.10**
10	0.53	**0.12**	**0.09**	**100**	**0.06**	**0.09**	**0.05**
cisplatin		**2a [μM]**		**cisplatin**		**2a [μM]**	
[μM]	**0.10**	**0.25**	**0.50**	**[μM]**	**0.10**	**0.25**	**0.50**

cisplatin [µM]				cisplatin [µM]			
0.10	*	0.56	0.40	1.00	*	0.76	0.33
0.32	*	0.39	0.32	3.20	*	0.44	0.25
1	0.91	0.11	0.16	10	*	0.23	0.12
3.2	0.37	0.07	0.07	32	*	0.04	0.03
10	0.33	0.02	0.07	100	0.07	0.03	0.07

cisplatin [µM]	2d [µM]			cisplatin [µM]	2d [µM]		
	0.50	1.00	3.20		0.50	1.00	3.20
0.10	0.50	0.42	0.39	1.00	0.77	*	*
0.32	0.70	0.52	0.34	3.20	*	0.81	0.89
1	0.59	0.46	0.23	10	0.76	0.50	0.31
3.2	0.21	0.20	0.14	32	*	0.27	0.18
10	0.18	0.16	0.08	100	0.10	0.08	0.19

The combination index analysis revealed synergistic interaction of **1h**, **2a**, and **2d** with cisplatin (CIs < 0.9). For **1h**, fraction affected at lower concentrations was frequently less than 0.20, and thus not eligible for analysis. Strong synergism as defined by CI values below 0.20 occurred mostly for **2a** which is in accordance with the observed higher shift factors for **2a** in comparison to **1h** and **2d**.

Enhancement of Cisplatin-Induced Apoptosis. Next, we examined if the increased

cisplatin cytotoxicity induced by **1h**, **2a**, or **2d** is mediated by increased apoptosis. Cal27

and Cal27CisR cells were treated for 48 h with 5 µM **1h**, 0.5 µM **2a**, or 3.2 µM **2d**. Then,

cisplatin was added for another 24 h in a concentration corresponding to IC_{50} values

from a 72 h MTT assay (Cal27: 3 µM, Cal27CisR: 25 µM), and the subG1 fraction of

nuclei was estimated by flow cytometry. Results are shown in Figure 6.
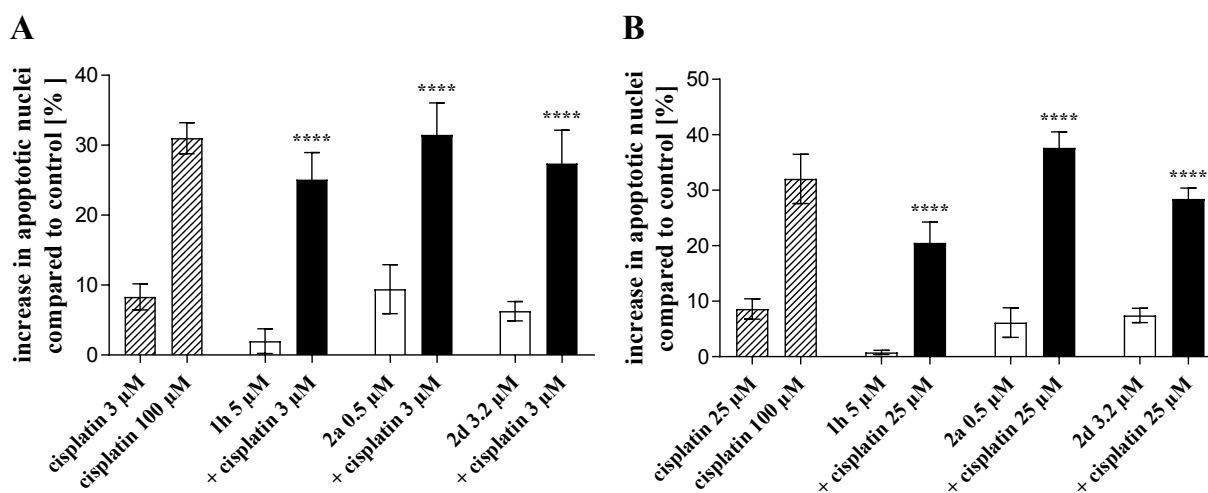
Figure 6. 1h, **2a**, and **2d** enhance cisplatin-induced apoptosis in Cal27 (A) and Cal27CisR

(B) cells. Cells were preincubated with 5 μM **1h**, 0.5 μM **2a,** or 3.2 μM **2d** for 48 h,

respectively. Cisplatin was added in an IC_{50} concentration for each cell line (Cal27 3 μM

(**A**), Cal27CisR 25 μM (**B**)). 100 μM cisplatin was used as a control for apoptosis induction.

After a further incubation period of 24 h, apoptosis was analysed by determining the sub-

G1 cell fractions by flow cytometry. The amount of apoptotic nuclei in the vehicle treated

control (0.05% DMSO) was subtracted from the compound treated samples. White bars

depict the incubation of cells with **1h**, **2a**, or **2d** only, whereas black bars show the effects

of the combination of **1h**, **2a**, or **2d** with cisplatin, respectively. Data are means ± SD, n =

3. Statistical analysis to compare the apoptosis induction by cisplatin alone and the

combination of cisplatin with **1h**, **2a**, or **2d,** respectively was performed using one-way

ANOVA (**** $p < 0.0001$).

2a and **2d** activated apoptosis in Cal27 and Cal27CisR as single treatment whereas **1h**

showed no effect on the subG1 population in both cell lines. The apoptosis induction of

2a and **2d** was similar to cisplatin (Cal27: cisplatin 8.32±0.71%, **2a** 9.42±1.56%, **2d** 6.27±0.70%, Cal27CisR: cisplatin 8.62±0.82%, **2a** 6.15±1.01%, **2d** 7.45±0.49%). The combination of **1h**, **2a**, or **2d** with cisplatin induced a significant increase in apoptosis in comparison to cisplatin alone in both cell lines. **2a** again turned out as the most potent compound. In Cal27 and Cal27CisR, **2a** plus cisplatin induced a 3.8-fold and 4.3-fold increase in apoptotic nuclei in comparison to a single treatment with cisplatin, respectively. In Cal27, apoptosis induction induced by **2a** plus 3 μM cisplatin was similar to 100 μM cisplatin alone (cisplatin 100 μM 31.0±1.11%, **2a** + cisplatin 3 μM 31.5±1.14%) whereas in Cal27CisR, **2a** plus 25 μM cisplatin gave a higher value than 100 μM cisplatin alone (cisplatin 100 μM 32.1±1.98%, **2a** + cisplatin 25 μM 37.7±0.79%).

In addition, the combination treatment markedly elevated caspase-3/7 activity in Cal27 and Cal27CisR. Caspase-3/7 activity was monitored by fluorescence image analysis. Results are shown in Figure 7.
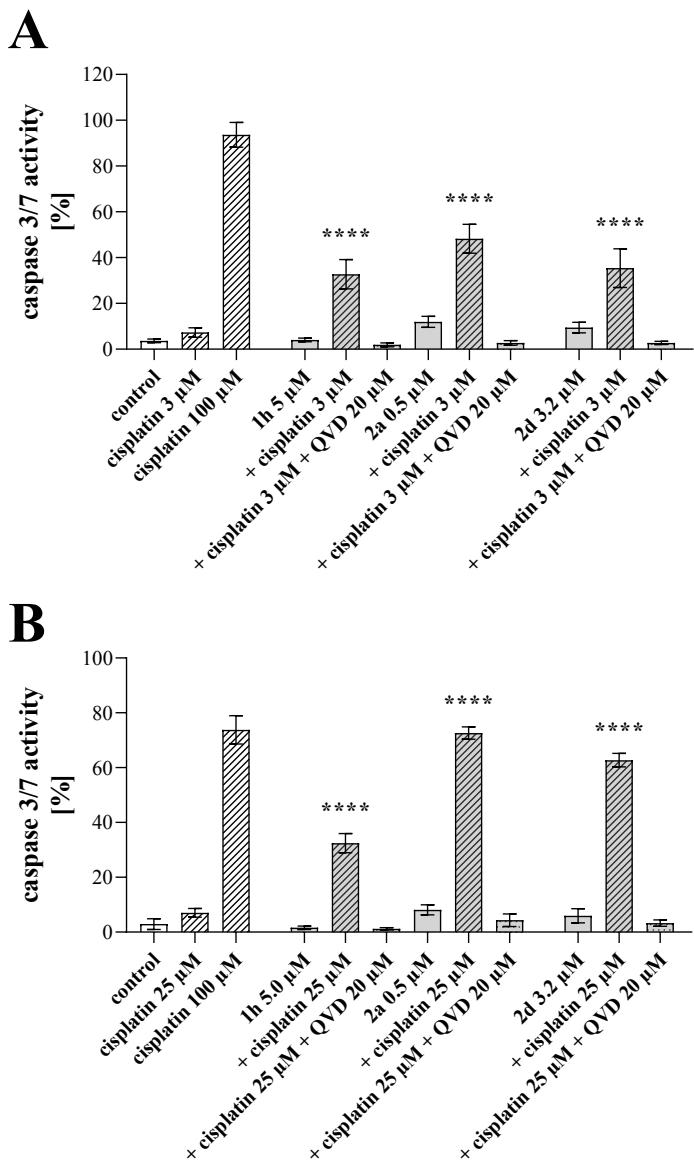
Figure 7. **1h, 2a,** and **2d** increase cisplatin-induced caspase-3/7 activation. Cal27 (A) and

Cal27CisR (B) were treated with the indicated concentrations of **1h, 2a,** and **2d** for 48h

prior to cisplatin addition (3 μM for Cal27 and 25 μM for Cal27CisR, respectively) or buffer

control and incubation for another 24 h. The pan caspase inhibitor QVD was used as control. The percentage of Cal27 cells (A) and Cal27CisR cells (B) with activated caspase-3/7 was calculated from the images (shown in Figure S1, Supporting Information). Data are means ± SD. One-way ANOVA was used to compare caspase 3/7 activation by cisplatin alone or the combination of cisplatin and **1h, 2a,** or **2d** (C, D) (**** $p < 0.0001$).

The combination of cisplatin with **1h**, **2a**, or **2d** led to a significant increase in caspase-3/7 activation in Cal27 and Cal27CisR. The incubation with **2a** and **2d** as single treatment showed an activation of caspase-3/7 in the range of cisplatin alone (Cal27: cisplatin 7.30±1.16%, **2a** 12.0±1.06%, **2d** 9.47±1.02%, Cal27CisR: cisplatin 7.05±0.90, **2a** 8.16±0.82, **2d** 5.96±1.17%), which is in accordance with results of subG1 analysis (apoptosis induction, Figure 6).

The increase in caspase 3/7 activation (Figure 7) and apoptosis induction (subG1, Figure 6) upon combination of cisplatin with **1h**, **2a**, or **2d** indicates synergism between cisplatin

and **1h**, **2a**, or **2d.** Adding the effects of the single treatments of cisplatin and of **1h**, **2a**, or

2d, respectively, does not reach the caspase 3/7 activation (Figure 7) or subG1-apoptosis

induction (Figure 6) of the combined cisplatin – HDACi (**1h**, **2a**, or **2d**) treatment, thus

supporting in addition to the combination index analysis a synergistic effect of HDACi **1h**,

2a, or **2d** and cisplatin.

2a in combination with cisplatin showed the highest activation of caspase-3/7 compared

to cisplatin alone (6.6-fold increase in Cal27; 10.3-fold increase in Cal27CisR), again

confirming the highest potency of **2a** among the novel HDACi. Caspase-3/7 activity of all

combination treatments was completely blocked by QVD suggesting specific activation of

caspases by the compound treatment.

Accumulation of acetylated tubulin and histone H3. Preincubation with **1h**, **2a**, or **2d**

showed a remarkable enhancement of cisplatin potency in caspase activation, apoptosis,

and cytotoxicity. To further confirm that the effects of **1h**, **2a**, or **2d** are mediated by HDAC

inhibition, the acetylation of histone H3 and α-tubulin was analyzed. Entinostat, nexturastat A, and vorinostat served as controls. Results are shown in Figure 8.
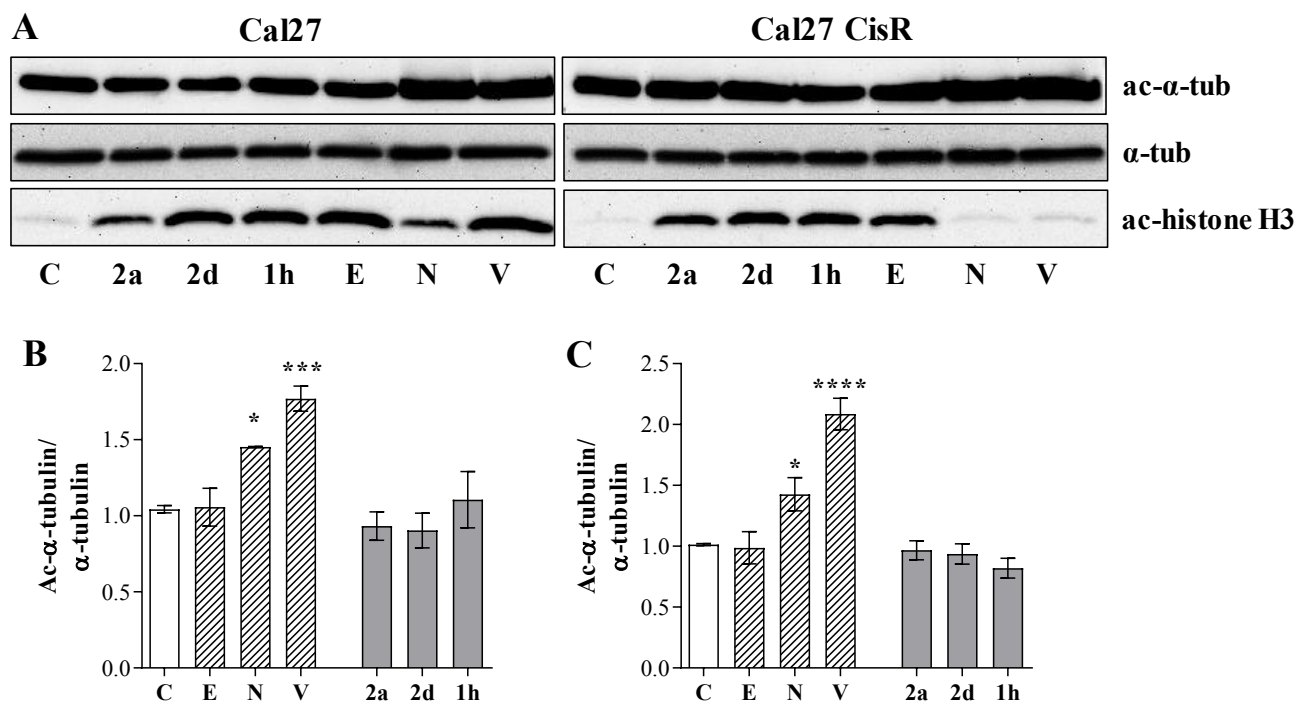
Figure 8. Compound-induced α-tubulin and histone H3 acetylation in Cal27 and Cal27CisR. **A** Representative immunoblot analysis of acetylated α-tubulin (ac-α-tub), α-tubulin (α-tub), and acetylated histone H3 (ac-histone H3). Cal27 and Cal27CisR were incubated for 24 h with vehicle as control (C, 0.05% DMSO), 0.5 μM **2a**, 3.2 μM **2d**, 5 μM **1h**, 1 μM entinostat (E), 1 μM nexturastat A (N), or 1 μM vorinostat (V), respectively. Densitometric analysis of tubulin acetylation in Cal27 (B) or Cal27CisR (C) was performed

by ImageJ software (NIH). All values have been normalized to α-tubulin. Statistical

analysis was performed using one-way ANOVA (* p<, *** p<, **** p<0.0001).

1h, **2a**, and **2d** did not influence the acetylation of α-tubulin after a 24 h incubation. Neither

did the HDAC1-3-selective HDACi entinostat (E). These results confirmed that **1h**, **2a**,

and **2d** showed no HDAC6 inhibition in both cell lines. In contrast, the pan-HDACi

vorinostat (V) and HDAC6-selective inhibitor nexturastat A (N) showed significant

acetylation of α-tubulin in Cal27 and Cal27CisR. However, **1h**, **2a**, and **2d** induced a

hyperacetylation of histone H3 similar to entinostat (E) and vorinostat (V) in Cal27 and

similar to entinostat (E) in Cal27 CisR. These observed effects underline class I HDAC

inhibition for all three compounds. Surprisingly, vorinostat induced only a slight increase

in histone H3 acetylation in Cal27CisR whereas the class I selective HDACi clearly

increase ac-histone H3.

CONCLUSIONS

This work describes efficient and versatile synthetic protocols for the preparation of peptoid-based HDACi with 2-aminoanilide groups as ZBG. To this end, we applied a convenient Ugi four-component reaction or straightforward submonomer pathways followed by the introduction of the ZBG to synthesize a library of peptoid-based HDACi. All synthesized compounds were screened for their inhibitory activity on HDAC1-3 and HDAC6, inhibition of cellular HDAC activity as well as cytotoxicity in the human ovarian cancer cell line A2780 and the human squamous carcinoma cell line Cal27. As expected, all compounds demonstrated inhibitory activity on recombinant HDAC1, 2, and/or 3 (class I) and were inactive against the class IIb isoform HDAC6. Docking studies were able to correctly predict the ligands' capabilities to inhibit the HDAC isoforms 1, 2, and 3. Western blot experiments confirmed the selective inhibition of class I HDACs in a cellular environment.

On the basis of anticancer activity and HDAC selectivity profile, compounds **1h**, **2a**, and **2d** were selected to investigate their activity against cisplatin-resistant cancer cells (Cal27CisR). Cisplatin resistance is a complex phenomenon and the major factor for

therapy failure besides toxic side effects of cisplatin. Mechanisms of cisplatin resistance include alterations in the cellular accumulation (decreased influx or increased efflux of cisplatin), intracellular detoxification (glutathione or metallothionein conjugation), and activated DNA damage repair or damage tolerance.[17,18] Combination therapies could be a promising approach to resensitize cancer towards cisplatin. It has already been shown by our group and others that a combination of an HDACi and cisplatin has a synergistic antitumor effect in hematological and solid tumors.[11,19,21,22] By leading to an open chromatin structure, HDACi increase the transcription of key genes involved in the regulation of cell proliferation, cell cycle, and apoptosis,[19,20,21] eventually resulting in the reestablishment of cisplatin sensitivity.

All three compounds were able to enhance the cisplatin-induced cytotoxicity and to resensitize the Cal27CisR cells towards cisplatin. The results from this study highlight once more the utility of class I selective HDACi in comparison to pan HDACi to resensitize cisplatin resistant cancer cells as we have recently shown with entinostat for high grade serous ovarian cancer cell lines (HGSOC).[21] HDAC1 selective inhibitors (**1h, 2d**), or

HDAC1, 2, and 3 inhibitors (**2a**) are all able to reverse cisplatin resistance, increase

caspase 3/7 activation and increase apoptosis in a synergistic manner. The most potent

HDACi, **2a** with nanomolar activity at HDAC1-3 and the highest cytotoxicity (higher than

vorinostat), showed the largest shift factors for reversing cisplatin resistance in a cellular

model of platinum resistance. We previously identified dual class I/class IIb inhibitors that

are able to enhance the cisplatin sensitivity in Cal27CisR cells.[11,22] Importantly, this study

provides for the first time evidence for the treatment of HNSCC that pan-HDAC inhibition

or dual class I/class IIb inhibition is not required for full reversal of cisplatin resistance.

Taken together, the concept of regaining chemosensitivity by applying epigenetic

modulators, here class I selective HDACi, is further corroborated by this study.

EXPERIMENTAL SECTION

Chemistry

General. Methyl 6-aminohexanoate hydrochloride,[23] 2-bromo-*N*-(4-

methoxybenzyl)acetamide,[24] *tert*-butyl (2-aminophenyl)carbamate,[25] *tert*-butyl (4-bromo-

2-nitrophenyl)carbamate,[26] *tert*-butyl (3-nitro-[1,1'-biphenyl]-4-yl)carbamate,[27] *tert*-butyl

(2-amino-4-fluorophenyl)carbamate,[28] and *tert*-butyl (3-amino-[1,1'-biphenyl]-4-

yl)carbamate[29] were prepared according to published procedures. All other chemicals

and solvents were obtained from commercial suppliers (Sigma-Aldrich, Acros Organics,

Carbolution Chemicals) and used as purchased without further purification. The progress

of all reactions was monitored by thin layer chromatography (TLC) using Merck precoated

silica gel plates (with fluorescence indicator UV_{254}). Components were visualized by

irradiation with ultraviolet light (254 nm) or staining in potassium permanganate solution.

Flash column chromatography was performed using prepacked silica cartridge with the

solvent mixtures specified in the corresponding experiment. Melting points (mp) were

taken in open capillaries on a Mettler FP 5 melting-point apparatus and are uncorrected.

Proton (^{1}H) and carbon (^{13}C) NMR spectra were recorded on a Bruker Avance 300, 500

or 600 using DMSO-d_6, MeOH-d_4 or $CDCl_3$ as solvents. Chemical shifts are given in parts

per million (ppm), relative to residual solvent peak for ^{1}H and ^{13}C. ^{1}H NMR signals marked

with an asterisk (*) correspond to peaks assigned to the minor rotamer conformation.

Elemental analysis was performed on a Perkin Elmer PE 2400 CHN elemental analyzer.

High resolution mass spectra (HRMS) analysis was performed on a UHR-TOF maXis 4G, Bruker Daltonics, Bremen by electrospray ionization (ESI). Analytical HPLC analysis were carried out on a Varian Prostar system equipped with a Prostar 410 (autosampler), 210 (pumps) and 330 (UV-detector) using a Phenomenex Luna 5u C18(2) 1.8 μm particle (250 mm × 4.6 mm) column, supported by Phenomenex Security Guard Cartridge Kit C18 (4.0 mm × 3.0 mm). UV absorption was detected at 254 nm with a linear gradient of 10% A to 100% A in 20 min using HPLC-grade water +0.1% TFA (solvent B) and HPLC-grade acetonitrile +0.1% TFA (solvent A) for elution at a flow rate of 1 mL/min. The purity of all final compounds was 95% or higher.

General procedures

General procedure for the synthesis of the compounds 1a-k and 2a-f.

The Boc-protected compound **4a-h, 7, 11a,b, and 13a-f** (0.1 mmol, 1 eq) was dissolved in a 15% solution of TFA in dichloromethane (5 mL) and stirred for 30 min at RT. After completion of the reaction, saturated sodium carbonate solution was added until no bubble formation was visible. The reaction solution was extracted with dichloromethane (3 x 15 mL) and washed with 1M sodium hydroxide (3 x 10 mL) and brine (3 x 10 mL). Subsequently, the collected organic extracts were dried over sodium sulfate and the solvent was removed under reduced pressure. The product was precipitated out of *n*-hexane and ethyl acetate.

General procedure for the synthesis of the compounds 3a-h and 12a-f.

A mixture of methyl 6-aminohexanoate hydrochloride (153 mg, 0.8 mmol, 1.2 eq), para-formaldehyde (25 mg, 0.8 mmol, 1.2 eq), triethylamine (116 µl, 0.8 mmol, 1.2 eq) and 150 mg crushed molecular sieves (MS, 4 Å) was stirred in dry methanol (2 mL, 0.5 M) for 30 min at RT. Subsequently, the appropriate carboxylic acid (1.0 mmol, 1.0 eq) and after further 10 min the isocyanide (1.0 mmol, 1.0 eq) were added and stirred for 24 h at RT. After completion of the reaction, the reaction mixture was filtered and the solvent was removed under reduced pressure. The crude products were purified by flash chromatography (prepacked silica cartridge, *n*-hexane-ethyl acetate, gradient: 100:00→50:50 in 30 min) and crystallized from ethyl acetate/*n*-hexane to yield the desired products **3a-h** and **12a-f**. The compound characterization data for **3a-e**, **3g, h** and **12d-f** were previously published.[11]

General procedure for the synthesis of the compounds 4a-h, 7, and 11a,b.

Lithium hydroxide monohydrate (92 mg, 2.2 mmol, 2 eq) was added to the appropriate ester **3a-h, 6,** or **10a,b** (1.1 mmol, 1 eq), dissolved in methanol (5 mL), and was stirred for 16 h at RT. After completion of the reaction, the solution was acidified with 1M HCl to a pH ~ 1. The reaction solution was extracted with ethyl acetate (3 x 20 mL) and washed with brine (3 x 20 mL). The solvent was removed under reduced pressure. The appropriate Boc-protected amine (0.9 mmol, 1 eq) was dissolved in CH$_2$Cl$_2$:DMF (1:1, v/v) and pyridine (149 µL, 1.8 mmol, 2 eq) was added. Subsequently, the appropriate carboxylic acid (1.1 mmol, 1.2 eq), DIC (170 µL, 1.1 mmol, 1.2 eq), and HOAt (150 mg, 1.1 mmol, 1.2 eq) were added and stirred for 24 h at RT. After completion of the reaction, the reaction solution was extracted with ethyl acetate (3 x 20 mL) and washed with

brine (3 x 20 mL). The combined organic extracts were dried over sodium sulfate. The crude products were purified by flash chromatography (prepacked silica cartridge, *n*-hexane-ethyl acetate, gradient: 100:00 → 40:60 in 30 min) and precipitated out of *n*-hexane and ethyl acetate.

General procedure for the synthesis of compounds 10a,b.

Compound **7** (984 mg, 2.5 mmol, 1 eq) was dissolved in 6 mL of a 20% TFA solution in dichloromethane. The solution was stirred for 2 h at RT. After completion of the reaction the solvent was removed under reduced pressure. The residue was treated with toluene (2 x 3 mL), which was subsequently removed under reduced pressure. The residue was partly (360 mg, 1.1 mmol, 1 eq) dissolved in DMF/CH_2Cl_2 (1:1, v/v, 5 mL). EDC·HCl (205 mg, 2.2 mmol, 2 eq) and DMAP (52 mg, 0.4 mmol, 0.4 eq) were added to the solution. Subsequently, the appropriate amine (1.1 mmol, 1 eq) was added and stirred for 16 h. After completion of the reaction, the solution was extracted with ethyl acetate (3 x 20 mL) and washed with brine (3 x 20 mL). The solvent was removed under reduced pressure. The crude products were purified by flash chromatography (prepacked silica cartridge, *n*-hexane-ethyl acetate, gradient 100:00→50:50 in 30 min) and the products were precipitated out of ethyl acetate and *n*-hexane.

General procedure for the synthesis of the compounds 13a-f.

Lithium hydroxide monohydrate (48 mg, 1.1 mmol, 2 eq) was added to the appropriate ester **12a-f** (0.6 mmol, 1 eq), dissolved in methanol (5 mL), and stirred for 16 h at RT. After completion of the reaction, the solution was acidified with 1M HCl to pH ~ 1 and extracted with ethyl acetate (3 x 20 mL). The solvent was removed under reduced pressure. To the appropriate carboxylic acid (0.6 mmol, 1 eq) in CH_2Cl_2:DMF (1:1, v/v), was added EDC·HCl (218 mg, 1.1 mmol, 2.4 eq) and DMAP (28 mg, 0.4 mmol, 0.4 eq) and stirred for 10 min. Subsequently, the appropriate Boc-

protected amine (0.6 mmol, 1 eq) was added to the reaction and stirred for further 24 h at RT. After completion of the reaction, the solution was extracted with ethyl acetate (3 x 20 mL) and washed with brine (3 x 20 mL). The crude products were purified by flash chromatography (prepacked silica cartridge, *n*-hexane-ethyl acetate, gradient: 100:00 → 40:60 in 30 min) and precipitated out of *n*-hexane and ethyl acetate.

Compound characterization data

N-{6-[(2-Aminophenyl)amino]-6-oxohexyl}-*N*-[2-(cyclohexylamino)-2-oxoethyl]benz-amide (1a). White solid; 52%; mp. 144 °C; t_R = 11.81 min, 98.5% purity; ^{1}H NMR (600 MHz, DMSO-d_6) δ 9.11/9.04* (s, 1H), 7.81 − 6.52 (m, 10H), 4.81/4.78* (s, 2H), 4.01*/3.74 (s, 2H), 3.56 − 3.16 (m, 3H), 2.33/2.22* (t, *J* = 7.0 Hz, 2H), 1.75 − 1.07 (m, 16H). ^{13}C NMR (151 MHz, DMSO-d_6) δ 171.2, 171.1, 167.1, 141.9, 136.9, 129.2, 129.2, 128.4, 128.3, 126.5, 126.4, 125.8, 125.4, 123.6, 116.3, 116.0, 51.5, 49.6, 47.7, 47.3, 45.9, 35.8, 35.6, 32.5, 32.3, 27.6, 26.4, 26.2, 25.7, 25.3, 24.9, 24.6, 24.5. HRMS (ESI) [M+H]+: 465.2868, Calcd. for $C_{27}H_{37}N_4O_3$: 465.2860.

N-{6-[(2-Aminophenyl)amino]-6-oxohexyl}-*N*-[2-(cyclohexylamino)-2-oxoethyl]-3,5-di-methylbenzamide (1b). White solid; 63%; mp. 85 °C; t_R = 12.58 min, 98.6% purity; ^{1}H NMR (600 MHz, DMSO-d_6) δ 9.09/9.02* (s, 1H), 7.78*/7.74 (d, *J* = 7.7 Hz, 1H), 7.16 − 6.51 (m, 7H), 4.81/4.78* (s, 2H), 3.98*/3.73 (s, 2H), 3.58 − 3.49 (m, 1H), 3.37 − 3.16 (m, 2H), 2.34 − 2.24 (m, 8H), 1.75 − 1.09 (m, 16H). ^{13}C NMR (151 MHz, DMSO-d_6) δ 171.13, 171.05, 167.2, 141.89, 141.86, 137.52, 137.51, 137.3, 136.8, 133.1, 130.4, 125.7, 125.7, 125.3, 125.2, 124.0 , 123.96, 123.6, 116.2, 115.9, 51.4, 51.3, 47.6, 47.6, 45.9, 45.8, 35.7, 35.6, 32.5, 32.3, 27.5, 27.3, 26.4, 26.2,

25.64, 25.62, 25.20, 25.15, 24.9, 24.8, 24.6, 24.5, 20.8. HRMS (ESI) [M+H]$^+$: 493.3178, Calcd.

for $C_{29}H_{40}N_4O_3$: 493.3173.

N-{6-[(2-Aminophenyl)amino]-6-oxohexyl}-N-[2-(benzylamino)-2-oxoethyl]-4-(dimethyl-

amino)benzamide (1c). White solid; 42%; mp. 139 °C; t_R = 9.30 min, 95.1% purity; ^{1}H NMR

(600 MHz, DMSO-d_6) δ 9.22 (bs, 1H), 8.54 (bs, 1H), 7.33 – 6.51 (m, 13H), 4.85 (s, 2H), 4.31 (d,

J = 5.7 Hz, 2H), 4.00 (m, 2H), 2.92 (s, 6H), 2.36 – 2.25 (m, 2H), 1.60 – 1.15 (m, 6H). ^{13}C NMR

(151 MHz, DMSO-d_6) δ 171.3, 171.1, 168.6, 150.9, 141.8, 139.4, 128.4, 128.3, 127.2, 126.8,

125.6, 125.2, 123.6, 116.1, 115.8, 110.9, 42.1, 40.1, 39.7, 35.6, 26.0, 25.5, 25.1. HRMS (ESI)

[M+H]$^+$: 516.2971, Calcd. for $C_{30}H_{38}N_5O_3$: 516.2969.

N-{6-[(2-Aminophenyl)amino]-6-oxohexyl}-N-[2-(benzylamino)-2-oxoethyl]-3,5-dimethyl-

benzamide (1d). White solid; 60%; mp. 147 °C; t_R = 12.83 min, 96.4% purity; ^{1}H NMR

(600 MHz, DMSO-d_6) δ 9.11/9.05* (s, 1H), 8.44 – 8.43 (m, 1H), 7.32 – 6.52 (m, 12H), 4.82/4.79*

(s, 2H), 4.34*/4.27 (d, J = 5.6 Hz, 2H), 4.08*/3.86 (s, 2H), 3.40 – 3.20 (m, 2H), 2.35 – 2.22 (m,

8H), 1.64 – 1.12 (m, 6H). ^{13}C NMR (151 MHz, DMSO-d_6) δ 171.1, 171.1, 168.2, 141.88, 141.85,

139.4, 139.2, 137.5, 137.4, 136.7, 136.5, 130.50, 130.45, 128.28, 128.25, 127.23, 127.15, 126.9,

126.7, 125.7, 125.3, 125.2, 124.04, 123.98, 123.6, 123.5, 116.2, 115.9, 51.4, 49.7, 47.5, 45.8, 42.2,

42.1, 35.7, 35.6, 27.6, 26.3, 26.1, 25.6, 25.2, 24.8, 20.8. HRMS (ESI) [M+H]$^+$: 501.2866, Calcd.

for $C_{30}H_{37}N_4O_3$: 501.2860.

N-{6-[(2-Aminophenyl)amino]-6-oxohexyl}-N-[2-(cyclohexylamino)-2-oxoethyl]-1-

naphthamide (1e). White solid; 80%; mp. 171 °C; t_R = 13.10 min, 98.4% purity; ^{1}H NMR (600

MHz, DMSO-d_6) δ 9.12*/8.98 (s, 1H), 8.21 – 6.51 (m, 12H), 4.83*/4.76 (s, 2H), 4.48 – 2.97 (m,

5H), 2.38*/2.13 (t, J = 7.4 Hz, 2H), 1.82 – 0.94 (m, 16H). ^{13}C NMR (151 MHz, DMSO-d_6) δ 171.1,

170.9, 170.02, 169.99, 166.9, 166.7, 141.9, 141.8, 134.8, 134.6, 133.0, 132.8, 129.2, 129.0, 128.6,

128.2, 128.1, 126.8, 126.5, 126.3, 125.7, 125.4, 125.28, 125.25, 125.2, 125.1, 124.7, 123.6, 123.5,

123.4, 116.2, 116.1, 115.88, 115.86, 50.9, 49.1, 47.7, 47.5, 46.7, 45.7, 35.7, 35.5, 32.5, 32.2, 27.5,

26.6, 26.3, 25.5, 25.23, 25.18, 25.1, 24.8, 24.6, 24.4. HRMS (ESI) [M+H]$^+$: 515.3021, Calcd. for

$C_{31}H_{39}N_4O_3$: 515.3017.

N-{6-[(2-Aminophenyl)amino]-6-oxohexyl}-N-[2-(benzylamino)-2-oxoethyl]-1-naphth-

amide (1f). White solid; 81%; mp. 148 °C; t_R = 12.73 min, 97.7% purity; ^{1}H NMR (600 MHz,

DMSO-d_6) δ 9.13*/8.98 (m, 1H), 8.58/8.23* (t, J = 5.9 Hz, 1H), 8.17 – 6.51 (m, 16H), 4.83*/4.76

(s, 2H), 4.52 – 3.01 (m, 6H), 2.39*/2.14 (t, J = 7.4 Hz, 2H), 1.75 – 0.97 (m, 6H). ^{13}C NMR (151

MHz, DMSO-d_6) δ 171.1, 170.9, 170.1, 170.0, 168.2, 167.9, 141.9, 141.8, 139.3, 139.0, 134.7,

134.5, 132.8, 131.5, 129.2, 128.6, 128.6, 128.3, 128.2, 127.3, 127.2, 126.84, 126.81, 126.5, 126.4,

125.7, 125.7, 125.33, 125.29, 125.24, 125.21, 123.59, 123.58, 123.5, 116.1, 115.9, 52.1, 50.9, 49.3,

47.0, 42.2, 42.0, 35.7, 35.5, 27.6, 26.6, 26.3, 25.5, 25.2, 24.8. HRMS (ESI) [M+H]$^+$: 523.2702,

Calcd. for $C_{32}H_{35}N_4O_3$: 523.2704.

N-{6-[(2-Amino-5-fluorophenyl)amino]-6-oxohexyl}-N-[2-(benzylamino)-2-oxoethyl]-4-

(dimethylamino)benzamide (1g). Greyish solid; 70%; mp. 76 °C; t_R = 10.38 min, 95.9% purity;

^{1}H NMR (600 MHz, DMSO-d_6) δ 9.08 (s, 1H), 8.45 (s, 1H), 7.33 – 6.64 (m, 12H), 4.77 (s, 2H),

4.31 (d, J = 5.7 Hz, 2H), 4.06 – 3.92 (m, 2H), 2.92 (s, 6H), 2.36 – 2.28 (m, 2H), 1.58 – 1.15 (m,

6H). ^{13}C NMR (151 MHz, DMSO-d_6) δ 171.3, 171.2, 168.6, 154.5, 153.0, 150.9, 139.4, 137.2,

128.4, 128.3, 127.2, 126.8, 124.4, 124.3, 123.0, 116.1, 116.0, 111.4, 111.2, 110.9, 110.6, 110.5, 110.4, 42.1, 40.1, 39.7, 35.8, 26.0, 25.0, 23.3. HRMS (ESI) [M+H]$^+$: 534.2882, Calcd. for C$_{30}$H$_{37}$FN$_5$O$_3$: 534.2875.

N-{6-[(4-Amino-[1,1'-biphenyl]-3-yl)amino]-6-oxohexyl}-N-[2-(benzylamino)-2-oxoethyl]-3,5-dimethylbenzamide (1h). Brown solid; 79%; mp. 92 °C; t_R = 14.68 min, 98.6% purity; ^{1}H NMR (600 MHz, DMSO-d_6) δ 9.18/9.11* (s, 1H), 8.47 – 8.39 (m, 1H), 7.56 – 6.80 (m, 16H), 5.03/5.00* (s, 2H), 4.34*/4.28 (d, J = 5.3 Hz, 2H), 4.09*/3.87 (s, 2H), 3.42 – 3.21 (m, 2H), 2.39 – 2.21 (m, 8H), 1.67 – 1.14 (m, 6H). ^{13}C NMR (151 MHz, DMSO-d_6) δ 171.28, 171.25, 171.14, 171.10, 168.21, 168.19, 141.4, 140.3, 139.4, 139.2, 137.4, 137.4, 136.7, 136.5, 130.5, 130.4, 128.8, 128.27, 128.25, 128.1, 127.2, 127.1, 126.9, 126.7, 126.0, 125.5, 124.04, 123.98, 123.9, 123.8, 123.28, 123.25, 116.2, 51.4, 49.7, 47.5, 45.8, 42.17, 42.07, 35.8, 35.7, 27.7, 26.3, 26.2, 25.6, 25.1, 24.8, 20.8. HRMS (ESI) [M+H]$^+$: 577.3175, Calcd. for C$_{36}$H$_{40}$N$_4$O$_3$: 577.3173.

N-{6-[(2-Aminophenyl)amino]-6-oxohexyl}-N-{2-[(4-methoxybenzyl)amino]-2-oxoethyl}-3,5-dimethylbenzamide (1i). Greyish solid; 57%; mp. 168 °C; t_R = 12.17 min, 96.7% purity; ^{1}H NMR (500 MHz, DMSO-d_6) δ 9.08/9.02* (s, 1H), 8.36 – 8.29 (m, 1H), 7.22 – 6.51 (m, 11H), 4.80/4.77* (s, 2H), 4.26*/4.20 (d, J = 4.7 Hz, 2H), 4.06*/3.83, 3.72 (s, 3H), 3.42 – 3.17 (m, 2H), 2.34 – 2.21 (m, 8H), 1.63 – 1.09 (m, 6H). ^{13}C NMR (126 MHz, DMSO-d_6) δ 171.0, 170.9, 168.0, 158.2, 141.8, 137.3, 130.4, 128.6, 128.4, 125.6, 125.1, 123.9, 123.6, 116.1, 115.8, 113.6, 55.0, 51.4, 49.6, 47.4, 45.7, 41.6, 41.5, 35.7, 35.6, 27.6, 26.3, 26.1, 25.6, 25.1, 24.8, 20.7. HRMS (ESI) [M+H]$^+$: 531.2968, Calcd. for C$_{31}$H$_{38}$N$_4$O$_4$: 531.2966.

N-{6-[(2-Aminophenyl)amino]-6-oxohexyl}-3,5-dimethyl-N-{2-[(4-methylbenzyl)amino]-2-oxoethyl}benzamide (1j). Brown solid; 91%; mp. 81 °C; t_R = 13.07 min, 96.1% purity; ^{1}H NMR (600 MHz, DMSO-d_6) δ 9.10/9.03* (s, 1H), 8.38 – 8.37 (m, 1H), 7.17 – 6.52 (m, 11H), 4.82 – 4.79 (m, 2H), 4.28*/4.22 (d, J = 5.2 Hz, 2H), 4.07*/3.84, 3.40 – 3.19 (m, 2H), 2.35 – 2.22 (m, 11H) 1.64 – 1.12 (m, 6H). ^{13}C NMR (151 MHz, DMSO-d_6) δ 171.1, 170.9, 168.1, 141.87, 141.85, 137.5, 137.4, 136.7, 136.4, 136.2, 135.9, 135.8, 130.49, 130.45, 128.8, 127.3, 127.2, 125.7, 125.3, 125.2, 124.03, 123.98, 123.58, 123.55, 116.2, 115.9, 51.4, 49.7, 47.5, 45.8, 41.92, 41.85, 35.7, 35.6, 27.6, 26.3, 26.1, 25.6, 25.2, 24.8, 20.8, 20.7. HRMS (ESI) [M+H]$^+$: 515.3021, Calcd. for $C_{31}H_{38}N_4O_3$: 515.3017.

N-{6-[(2-Aminophenyl)amino]-6-oxohexyl}-N-{2-[(3,5-dimethylbenzyl)amino]-2-oxo-ethyl}-3,5-dimethylbenzamide (1k). White solid; 82%; mp. 83 °C; t_R = 13.82 min, 96.0% purity; ^{1}H NMR (600 MHz, DMSO-d_6) δ 9.10/9.03* (s, 1H), 8.36 – 8.35 (m, 1H), 7.17 – 6.52 (m, 10H), 4.81/4.78* (s, 2H), 4.25*/4.19 (d, J = 4.2 Hz, 2H), 4.07*/3.84 (s, 2H), 3.39 – 3.21 (m, 2H), 2.34 – 2.21 (m, 14H), 1.63 – 1.12 (m, 6H). ^{13}C NMR (151 MHz, DMSO-d_6) δ 171.1, 170.9, 168.1, 141.9, 139.2, 138.9, 137.5, 137.4, 137.23, 137.17, 136.7, 136.5, 130.5, 130.4, 128.3, 128.1, 125.7, 125.3, 125.2, 125.0, 124.0, 123.6, 123.5, 116.2, 115.9, 51.4, 49.7, 47.5, 45.7, 42.2, 42.0, 35.7, 35.6, 27.6, 26.3, 26.2, 25.6, 25.2, 24.8, 20.9, 20.8, 20.7. HRMS (ESI) [M+H]$^+$: 529.3178, Calcd. for $C_{32}H_{40}N_4O_3$: 529.3173.

N-{4-[(2-Aminophenyl)carbamoyl]benzyl}-N-[2-(benzylamino)-2-oxoethyl]-4-(dimethyl-amino)benzamide (2a). White solid; 82%; mp. 128 °C; t_R = 9.98 min, 95.8% purity; ^{1}H NMR (500 MHz, DMSO-d_6) δ 9.64 (s, 1H), 8.47 – 8.41 (m, 1H), 8.00 – 6.60 (m, 17H), 4.88 (s, 2H), 4.73

(s, 2H), 4.33 (d, J = 5.7 Hz, 2H), 3.93 (s, 2H), 2.94 (s, 6H). ^{13}C NMR (126 MHz, DMSO-d_6)

δ 171.7, 168.1, 165.0, 151.2, 143.0, 141.0, 139.2, 133.5, 128.5, 128.2, 128.0, 127.2, 126.8, 126.6,

126.4, 123.3, 116.2, 116.1, 110.9, 42.1. HRMS (ESI) [M+H]$^+$: 536.2654, Calcd. for C$_{32}$H$_{34}$N$_5$O$_3$:

536.2656.

N-{4-[(2-Aminophenyl)carbamoyl]benzyl}-N-[2-(benzylamino)-2-oxoethyl]-3,5-dimethyl-

benzamide (2b). White solid; 74%; mp. 110 °C; t_R = 13.08 min, 95.2% purity; ^{1}H NMR

(600 MHz, DMSO-d_6) δ 9.67 − 9.66 (m, 1H), 8.46*/8.42 (t, J = 5.8 Hz, 1H), 7.99 − 6.59 (m, 16H),

4.90 (s, 2H), 4.73/4.60* (s, 2H), 4.34*/4.29 (d, J = 5.8 Hz, 2H), 4.01*/3.81 (s, 2H), 2.26 − 2.25 (m,

6H). ^{13}C NMR (151 MHz, DMSO-d_6) δ 171.61, 171.59, 167.8, 167.6, 165.1, 164.9, 143.2, 143.1,

140.8, 140.4, 139.3, 139.1, 137.64, 137.61, 136.0, 135.9, 133.7, 133.6, 130.9, 130.8, 128.32,

128.28, 128.2, 128.1, 127.6, 127.24, 127.16, 126.9, 126.83, 126.78, 126.7, 126.5, 124.14, 124.08,

123.31, 123.26, 116.3, 116.1, 53.2, 51.0, 48.7, 47.4, 42.2, 42.1, 28.0, 20.8. HRMS (ESI) [M+H]$^+$:

536521.2551, Calcd. for C$_{32}$H$_{32}$N$_4$O$_3$: 521.2547.

N-{4-[(2-Aminophenyl)carbamoyl]benzyl}-N-[2-(benzylamino)-2-oxoethyl]nicotinamide

(2c). White solid; 75%; mp. 120 °C; t_R = 8.87 min, 95.4% purity; ^{1}H NMR (600 MHz, DMSO-d_6)

δ 9.68 (s, 1H), 8.69 − 6.59 (m, 18H), 4.90 (s, 2H), 4.75/4.65* (s, 2H), 4.35*/4.26 (d, J = 5.4 Hz,

2H), 4.09*/3.89 (s, 2H). ^{13}C NMR (151 MHz, DMSO-d_6) δ 169.5, 169.3, 167.6, 167.4, 165.0,

164.9, 150.7, 150.5, 147.4, 147.1, 143.2, 140.4, 140.1, 139.3, 138.8, 134.5, 133.8, 133.6, 132.0,

131.7, 128.33, 128.30, 128.25, 128.0, 127.7, 127.22, 127.17, 126.9, 126.8, 126.7, 126.5, 123.6,

123.4, 123.32, 123.25, 116.3, 116.1, 53.4, 51.2, 49.1, 48.2, 42.3, 42.1. HRMS (ESI) [M+H]$^+$:

494.2192, Calcd. for C$_{29}$H$_{28}$N$_5$O$_3$: 494.2187.

N-{4-[(4-Amino-[1,1'-biphenyl]-3-yl)carbamoyl]benzyl}-N-[2-(benzylamino)-2-oxoethyl]-3,5-dimethylbenzamide (2d). White/rose solid; 65%; mp. 124 °C; t_R = 15.75 min, 97.6% purity; ^{1}H NMR (600 MHz, DMSO-d_6) δ 9.76*/9.75 (s, 1H), 8.47*/8.43 (t, J = 5.6 Hz, 1H), 8.03 − 6.87 (m, 20H), 5.11 (s, 2H), 4.74/4.62* (s, 2H), 4.34*/4.29 (d, J = 5.7 Hz, 2H), 4.02*/3.82 (s, 2H), 2.25 (s, 6H). ^{13}C NMR (151 MHz, DMSO-d_6) δ 171.62, 171.60, 167.8, 167.7, 165.2, 165.1, 142.84, 142.77, 140.9, 140.2, 139.3, 139.1, 137.6, 136.0, 135.9, 133.7, 133.5, 130.9, 130.8, 128.8, 128.32, 128.28, 128.25, 128.1, 128.1, 127.6, 127.3, 127.2, 126.9, 126.84, 126.78, 126.0, 125.5, 124.82, 124.76, 124.7, 124.2, 124.1, 123.6, 123.5, 116.5, 53.2, 51.0, 48.7, 47.5, 42.2, 42.1, 20.8. HRMS (ESI) [M+H]$^+$: 597.2859, Calcd. for $C_{38}H_{37}N_4O_3$: 597.2860.

N-{4-[(4-Amino-[1,1'-biphenyl]-3-yl)carbamoyl]benzyl}-N-[2-(benzylamino)-2-oxoethyl]-4-(dimethylamino)benzamide (2e). Rose solid; 75%; mp. 122 °C; t_R = 12.75 min, 95.8% purity; ^{1}H NMR (600 MHz, DMSO-d_6) δ 9.74 (s, 1H), 8.48 (bs, 1H), 8.02 − 6.65 (m, 21H), 5.10 (s, 2H), 4.73 (bs, 2H), 4.32 (d, J = 5.8 Hz, 2H), 3.93 (bs, 2H), 2.94 (s, 6H). ^{13}C NMR (151 MHz, DMSO-d_6) δ 171.8, 168.2, 165.2, 151.3, 142.8, 141.1, 140.2, 139.3, 133.5, 128.8, 128.6, 128.3, 128.1, 127.3, 126.9, 126.0, 125.5, 124.8, 124.7, 123.6, 116.5, 111.0, 42.1. HRMS (ESI) [M+H]$^+$: 612.2967, Calcd. for $C_{38}H_{37}N_5O_3$: 612.2969.

N-{4-[(2-Amino-5-fluorophenyl)carbamoyl]benzyl}-N-[2-(benzylamino)-2-oxoethyl]-3,5-dimethylbenzamide (2f). White solid; 88%; mp. 211 °C; t_R = 13.60 min, 95.1% purity; ^{1}H NMR (600 MHz, DMSO-d_6) δ 9.68*/9.66 (s, 1H), 8.46*/8.42 (t, J = 5.7 Hz, 1H), 7.98 − 6.77 (m, 15H), 4.85 (s, 2H), 4.74/4.61* (s, 2H), 4.34*/4.29 (d, J = 5.7 Hz, 2H), 4.01*/3.81 (s, 2H), 2.25 (s, 6H).

¹³C NMR (151 MHz, DMSO-d_6) δ 171.6, 167.8, 167.6, 165.2, 165.0, 154.6, 153.0, 141.0, 140.7, 139.3, 139.1, 139.0, 138.9, 137.64, 137.62, 136.0, 135.8, 133.5, 133.3, 130.9, 130.8, 128.32, 128.28, 128.2, 128.1, 127.7, 127.3, 127.2, 126.91, 126.88, 126.78, 124.14, 124.09, 116.62, 116.57, 112.7, 112.6, 112.44, 112.35, 112.3, 112.2, 53.2, 51.0, 48.7, 47.5, 42.2, 42.1, 20.8. HRMS (ESI) [M+H]⁺: 539.2450, Calcd. for $C_{32}H_{32}FN_4O_3$: 539.2453.

Methyl 6-{*N*-[2-(benzylamino)-2-oxoethyl]-1-naphthamido}hexanoate (3f). White solid; 90%; mp. 91 °C; ¹H NMR (600 MHz, DMSO-d_6) δ 8.57/8.22* (t, *J* = 5.9 Hz, 1H), 8.23 – 7.05 (m, 12H), 4.48 – 2.99 (m, 9H), 2.37*/2.06 (t, *J* = 7.3 Hz, 2H), 1.70 – 0.91 (m, 6H). ¹³C NMR (151 MHz, DMSO-d_6) δ 173.4, 173.1, 170.0, 168.2, 167.9, 139.3, 139.0, 134.7, 134.5, 133.0, 132.8, 129.2, 128.9, 128.6, 128.6, 128.3, 128.2, 128.1, 127.24, 127.17, 126.9, 126.8, 126.5, 126.4, 125.3, 124.6, 125.20, 125.17, 123.6, 123.5, 51.2, 51.1, 50.9, 49.2, 47.1, 45.6, 42.2, 42.0, 33.2, 32.8, 27.3, 26.4, 26.0, 25.1, 24.3, 23.7. Anal. Calcd. for $C_{27}H_{30}N_2O_4$: C 72.62, H 6.77, N 6.27. Found: C 72.55, H 6.88, N 6.14.

tert-Butyl [2-(6-{*N*-[2-(cyclohexylamino)-2-oxoethyl]benzamido}hexanamido)phenyl]-carbamate (4a). White solid; 71%; mp. 94 °C; t_R = 17.92 min, 96.6% purity; ¹H NMR (600 MHz, DMSO-d_6) δ 9.44/9.37* (s, 1H), 8.34/8.30* (s, 1H), 7.80 – 7.76 (m, 1H), 7.53 – 7.05 (m, 8H), 4.01*/3.74 (s, 2H), 3.57 – 3.51 (m, 1H), 3.38 – 3.16 (m, 2H), 2.37/2.25* (t, *J* = 7.0 Hz, 2H), 1.76 – 1.08 (m, 25H).¹³C NMR (151 MHz, DMSO-d_6) δ 171.7, 171.5, 170.9, 170.8, 167.0, 166.8, 153.1, 153.0, 136.8, 136.6, 131.1, 131.0, 129.7, 129.6, 129.1, 128.3, 128.2, 126.5, 126.3, 125.0, 124.8, 123.8, 123.6, 79.3, 51.4, 49.6, 47.6, 47.3, 45.8, 45.7, 35.9, 35.7, 32.4, 32.2, 28.1, 27.5, 26.4, 26.2,

26.0, 25.9, 25.5, 25.2, 25.14, 25.05, 24.7, 24.54, 24.45, 24.29. HRMS (ESI) [M+H]$^+$: 565.3386,

Calcd. for $C_{32}H_{45}N_4O_5$: 565.3384.

tert-Butyl [2-(6-{N-[2-(cyclohexylamino)-2-oxoethyl]-3,5-dimethylbenzamido}hexan-ami-do)phenyl]carbamate (4b). White solid; 70%; mp. 88 °C; t_R = 19.45 min, 97.5% purity; ^{1}H NMR (500 MHz, DMSO-d_6) δ 9.41/9.34* (s, 1H), 8.30/8.27* (s, 1H), 7.74 − 7.69 (m, 1H), 7.54 − 6.92 (m, 7H), 3.99*/3.73 (s, 2H), 3.60 − 3.50 (m, 1H), 3.37 − 3.17 (m, 2H), 2.37 − 2.24 (m, 8H), 1.76 − 1.10 (m, 25H). ^{13}C NMR (126 MHz, DMSO-d_6) δ 171.6, 171.4, 170.9, 167.0, 166.8, 153.0, 137.3, 137.2, 136.8, 136.6, 131.0, 130.3, 129.6, 124.9, 124.7, 123.9, 123.7, 123.5, 79.2, 51.3, 49.4, 47.5, 47.1, 45.7, 35.8, 32.1, 28.0, 27.4, 26.2, 25.9, 25.4, 25.1, 24.9, 24.6, 24.3, 20.6. HRMS (ESI) [M+H]$^+$: 593.3700, Calcd. for $C_{34}H_{49}N_4O_5$: 593.3697.

tert-Butyl [2-(6-{N-[2-(benzylamino)-2-oxoethyl]-4-(dimethylamino)benzamido}hexan-amido)phenyl]carbamate (4c). White solid; 56%; mp. 94 °C; t_R = 13.97 min, 95.2% purity; ^{1}H NMR (600 MHz, DMSO-d_6) δ 9.43 (s, 1H), 8.45 (bs, 1H), 8.33 (s, 1H), 7.55 − 6.64 (m, 13H), 4.31 (d, J = 5.8 Hz, 2H), 3.98 (bs, 2H), 3.35 − 3.33 (m, 2H), 2.38 − 2.29 (m, 2H), 1.59 − 1.25 (m, 15H). ^{13}C NMR (151 MHz, DMSO-d_6) δ 171.5, 171.2, 168.5, 153.0, 150.9, 139.3, 131.0, 129.6, 128.4, 128.3, 128.1, 127.1, 126.7, 124.9, 124.7, 123.7, 123.5, 123.0, 110.8, 79.2, 42.1, 35.8, 33.5, 28.0, 25.8, 24.8, 24.1. HRMS (ESI) [M+H]$^+$: 616.3496, Calcd. for $C_{36}H_{46}N_5O_5$: 616.3493.

tert-Butyl [2-(6-{N-[2-(benzylamino)-2-oxoethyl]-3,5-dimethylbenzamido}hexanamido)-phenyl]carbamate (4d). White solid; 61%; mp. 73 °C; t_R = 17.40 min, 95.4% purity; ^{1}H NMR (600 MHz, DMSO-d_6) δ 9.44/9.38* (s, 1H), 8.42 (t, J = 5.7 Hz, 1H), 8.34/8.30* (s, 1H), 7.53 − 6.92

(m, 12H), 4.33*/4.27 (d, J = 5.5 Hz, 2H), 4.07*/3.85 (s, 2H), 3.40 – 3.18 (m, 2H), 2.38 – 2.21 (m, 2H), 1.68 – 1.12 (m, 15H). ^{13}C NMR (151 MHz, DMSO-d_6) δ 171.7, 171.5, 171.13, 171.08, 168.2, 153.1, 153.0, 139.4, 139.2, 137.4, 137.4, 136.7, 136.5, 131.1, 131.0, 130.49, 130.46, 129.7, 129.6, 128.28, 128.25, 127.24, 127.16, 126.9, 126.7, 125.0, 124.8, 124.01, 123.98, 123.8, 123.6, 79.3, 79.3, 51.4, 49.7, 47.5, 45.8, 42.2, 42.1, 35.9, 35.8, 28.1, 27.6, 26.3, 26.0, 25.5, 25.0, 24.8, 24.7, 20.8. HRMS (ESI) [M+H]$^+$: 601.3385, Calcd. for $C_{36}H_{45}N_4O_5$: 601.3384.

***tert*-Butyl [2-(6-{*N*-[2-(cyclohexylamino)-2-oxoethyl]-1-naphthamido}hexanamido)-phenyl]carbamate (4e).** White solid; 57%; mp. 89 °C; t_R = 19.94 min, 96.2% purity; ^{1}H NMR (600 MHz, DMSO-d_6) δ 9.47*/9.30 (s, 1H), 8.36*/8.26 (s, 1H), 8.19 – 7.04 (m, 12H), 4.47 – 2.97 (m, 5H), 2.42*/2.16 (t, J = 7.2 Hz, 2H), 1.81 – 0.94 (m, 25H). ^{13}C NMR (151 MHz, DMSO-d_6) δ 171.7, 171.5, 170.00, 169.98, 166.8, 166.7, 153.1, 153.0, 134.8, 134.5, 133.0, 132.8, 131.1, 131.0, 129.7, 129.6, 129.2, 129.0, 128.6, 128.6, 128.3, 128.1, 126.8, 126.5, 126.3, 125.4, 125.2, 125.1, 125.01, 124.99, 124.9, 124.8, 124.7, 123.9, 123.8, 123.6, 123.4, 79.4, 79.3, 50.9, 49.1, 47.7, 47.5, 46.7, 45.7, 36.0, 35.7, 32.5, 32.2, 28.1, 28.0, 27.5, 26.6, 26.2, 25.4, 25.2, 25.10, 25.06, 24.61, 24.56, 24.4. HRMS (ESI) [M+H]$^+$: 615.3550, Calcd. for $C_{36}H_{47}N_4O_5$: 615.3541.

***tert*-Butyl [2-(6-{*N*-[2-(benzylamino)-2-oxoethyl]-1-naphthamido}hexanamido)phenyl]carbamate (4f).** White solid; 71%; mp. 93 °C; t_R = 18.66 min, 96.2% purity; ^{1}H NMR (600 MHz, DMSO-d_6) δ 9.47*/9.31 (s, 1H), 8.58/8.23* (t, J = 5.9 Hz), 8.36*/8.27 (s, 1H), 8.16 – 7.04 (m, 17H), 4.51 – 3.02 (m, 6H), 2.42*/2.15 (t, J = 7.2 Hz, 2H), 1.75 – 0.98 (m, 15H). ^{13}C NMR (151 MHz, DMSO-d_6) δ 171.8, 171.5, 170.1, 170.0, 168.2, 167.9, 153.1, 153.0, 139.3, 139.0, 134.7, 134.5, 133.0, 132.8, 131.1, 131.0, 129.7, 129.6, 129.2, 128.9, 128.7, 128.6, 128.3, 128.2, 128.2, 127.3,

127.2, 126.9, 126.8, 126.5, 126.4, 125.3, 125.19, 125.17, 125.0, 124.9, 124.8, 124.6, 123.9, 123.8,

123.6, 123.5, 79.4, 79.3, 50.9, 49.4, 47.1, 45.8, 42.2, 42.1, 36.0, 35.7, 28.1, 28.0, 27.6, 26.6, 26.2,

25.4, 25.1, 24.6. HRMS (ESI) [M+H]+: 565.3386, Calcd. for $C_{32}H_{45}N_4O_5$: 565.3384.

tert-Butyl [2-(6-{N-[2-(benzylamino)-2-oxoethyl]-4-dimethylamino}benzamido)hexan-amido]-4-fluorophenylcarbamate (4g). White solid; 70%; mp. 85 °C; t_R = 14.65 min, 95.0% purity; ^{1}H NMR (600 MHz, DMSO-d_6) δ 9.36 (s, 1H), 8.51 – 8.38 (m, 2H), 7.50 – 6.63 (m, 12H), 4.31 (d, J = 5.6 Hz, 2H), 3.98 (bs, 2H), 2.92 (s, 6H), 2.38 – 2.30 (m, 2H), 1.58 – 1.17 (m, 15H). ^{13}C NMR (151 MHz, DMSO-d_6) δ 171.6, 171.3, 168.5, 159.2, 157.3, 153.3, 150.9, 139.3, 131.9, 128.3, 128.17, 127.18, 126.7, 126.2, 125.7, 123.0, 110.9, 110.7, 79.3, 42.1, 36.0, 28.0, 27.2, 25.8, 24.7. HRMS (ESI) [M+H]+: 634.3410, Calcd. for $C_{35}H_{45}FN_5O_5$: 634.3399.

tert-Butyl [3-(6-{N-[2-(benzylamino)-2-oxoethyl]-3,5-dimethylbenzamido}hexanamido)-[1,1'-biphenyl]-4-yl]carbamate (4h). Rose solid; 68%; mp. 138 °C; ^{1}H NMR (600 MHz, DMSO-d_6) δ 9.52/9.45* (s, 1H), 8.47 – 8.43 (m, 2H), 7.77 – 6.92 (m, 16H), 4.34*/4.27 (d, J = 5.2 Hz, 2H), 4.09*/3.86 (s, 2H), 3.41 – 3.22 (m, 2H), 2.42 – 2.20 (m, 2H), 1.67 – 1.15 (m, 15H). ^{13}C NMR (151 MHz, DMSO-d_6) δ 171.9, 171.7, 171.1, 171.10, 168.20, 168.17, 153.1, 153.0, 139.4, 139.2, 137.4, 136.7, 136.5, 135.6, 130.5, 130.4, 129.9, 129.0, 128.27, 128.25, 127.3, 127.24, 127.16, 126.9, 126.7, 126.3, 124.02, 123.98, 123.84, 123.84, 123.2, 122.8, 79.5, 51.4, 49.7, 47.6, 45.8, 42.2, 42.1, 36.0, 35.9, 28.1, 27.7, 26.3, 26.0, 25.5, 25.0, 24.7, 20.8. HRMS (ESI) [M+H]+: 677.3702, Calcd. for $C_{41}H_{49}N_4O_5$: 677.3697. Anal. Calcd. for $C_{41}H_{48}N_4O_5$: C 72.76, H 7.15, N 8.28. Found: C 72.52, H 7.36, N 7.99.

Methyl 6-(*N*-{2-[(4-methoxybenzyl)amino]-2-oxoethyl}-3,5-dimethylbenzamido)-hexa-noate

(6). Methyl 6-aminohexanoate hydrochloride (1.8 g, 9.9 mmol, 1 eq) was dissolved in dichloro-methane (30 mL) at 0 °C and triethylamine (2.75 ml, 19.8 mmol, 2 eq) was added. Subsequently, 2-bromo-*N*-(4-methoxybenzyl)acetamide (2.56 g, 9.9 mmol, 1 eq) was added and stirred for 16 h at RT. After completion of the reaction the solution was extracted with dichloromethane (3 x 30 mL) and washed with water (3 x 30 mL) and brine (3 x 30 mL). The secondary amine **5** (2.26 g, 7.0 mmol, 1.2 eq) was directly used in a reaction with pyridine (566 µL, 7.0 mmol, 1.2 eq) in dichloromethane at 0 °C. Subsequently, 3,5-dimethylbenzoyl-chloride (864 µL, 5.8 mmol, 1 eq) was added and stirred for 16 h at RT. The reaction solution was extracted with dichloromethane (3 x 20 mL) and washed with water (3 x 20 mL) and 1M hydrochloric acid (3 x 10 mL). The product **6** was precipitated out of ethyl acetate and *n*-hexane. White solid; 57%; mp. 59 °C; ^{1}H NMR (600 MHz, DMSO-d_6) δ 8.35 – 8.34 (m, 1H), 7.21 – 6.85 (m, 7H), 4.25*/4.19 (d, J = 5.4 Hz, 2H), 4.04*/3.81 (s, 2H), 3.72 (s, 3H), 3.59/3.56* (s, 3H), 3.36 – 3.15 (m, 2H), 2.33 – 2.18 (m, 8H), 1.56 – 1.04 (m, 6H). ^{13}C NMR (151 MHz, DMSO-d_6) δ 173.3, 173.2, 171.1, 168.0, 158.3, 158.2, 137.4, 137.4, 136.7, 136.5, 131.4, 131.2, 130.5, 128.6, 128.5, 124.0, 113.7, 55.1, 51.4, 51.2, 49.5, 47.5, 45.6, 41.6, 41.5, 33.2, 33.0, 27.3, 26.1, 25.8, 25.3, 24.2, 23.8, 20.8. Anal. Calcd. for $C_{26}H_{34}N_2O_5$: C 68.70, H 7.54, N 6.16. Found: C 68.67, H 7.75, N 6.23.

***tert*-Butyl {2-[6-(*N*-{2-[(4-methoxybenzyl)amino]-2-oxoethyl}-3,5-dimethylbenzamido)-hexanamido]phenyl}carbamate (7).** White solid; 60%; mp. 77 °C; t_R = 18.48 min, 99.5% purity; ^{1}H NMR (600 MHz, DMSO-d_6) δ 9.44/9.38* (s, 1H), 8.35 – 8.30 (m, 2H), 7.53 – 6.85 (m, 11H), 4.26*/4.19 (d, J = 4.8 Hz, 2H), 4.05*/3.82 (s, 2H), 3.71 (s, 3H), 3.39 – 3.20 (m, 2H), 2.38 – 2.21 (m, 8H), 1.64 – 1.12 (m, 15H). ^{13}C NMR (151 MHz, DMSO-d_6) δ 171.7, 171.6, 171.11, 171.07,

168.02, 167.99, 158.3, 158.2, 153.1, 137.44, 137.40, 136.7, 136.5, 131.3, 131.2, 131.1, 130.5, 129.7, 128.7, 128.5, 125.0, 124.8, 124.0, 123.8, 123.6, 113.7, 79.33, 79.31, 55.0, 51.4, 49.7, 47.5, 45.8, 41.63, 41.55, 35.9, 35.8, 28.1, 27.6, 26.3, 26.0, 25.5, 25.0, 24.7, 20.8. HRMS (ESI) $[M+H]^+$: 631.3489, Calcd. for $C_{36}H_{46}N_4O_6$: 631.3490.

Methyl 6-{*N*-[2-(*tert*-butoxy)-2-oxoethyl]-3,5-dimethylbenzamido}hexanoate (9). To a solution of methyl 6-aminohexanoate hydrochloride (2.9 g, 16.1 mmol, 1 eq) in tetrahydrofurane (30 mL), triethylamine (4.5 mL, 32.2 mmol, 2 eq) was added and stirred for 10 min at RT. Subsequently, *tert*-butyl bromoacetate (2.4 mL, 16.1 mmol, 1 eq) was added and stirred for further 16 h at RT. After completion of the reaction, the solvent was removed under reduced pressure. The crude product **8** (3.76 g, 14.5 mmol, 1.2 eq) was dissolved in dichloromethane (20 mL) at 0 °C. Pyridine (1.2 mL, 14.5 mmol, 1.2 eq) and 3,5-dimethyl-benzoylchloride (1.8 mL, 12.1 mmol, 1 eq) were added and the solution was stirred for 18 h at RT. The solvent was removed under reduced pressure. The crude product was purified by flash chromatography (prepacked silica cartridge, *n*-hexane-ethyl acetate, gradient: 100:00 → 50:50 in 30 min). Yellowish oil; 57%; t_R = 19.68 min, 97.6% purity; ^{1}H NMR (600 MHz, CDCl$_3$) δ 6.96 – 6.92 (m, 3H), 4.04/3.78* (s, 2H), 3.61*/3.59 (s, 3H), 3.45*/3.22 (t, *J* = 7.5 Hz, 2H), 2.30 – 2.16 (m, 8H), 1.66 – 1.10 (m, 15H). ^{13}C NMR (151 MHz, CDCl$_3$) δ 174.0, 173.7, 172.4, 172.4, 168.7, 168.3, 138.0, 136.3, 136.0, 131.02, 130.98, 124.2, 124.0, 82.1, 81.7, 51.9, 51.4, 49.9, 47.3, 46.5, 33.9, 33.7, 28.1, 28.1, 28.0, 26.8, 26.5, 25.9, 24.7, 24.3, 21.2. HRMS (ESI) $[M+H]^+$: 392.2434, Calcd. for $C_{22}H_{34}NO_5$: 392.2431.

Methyl 6-(3,5-dimethyl-*N*-{2-[(4-methylbenzyl)amino]-2-oxoethyl}benzamido)hexanoate (10a). White solid; 71%; mp. 78 °C; ^{1}H NMR (600 MHz, DMSO-*d*$_6$) δ 8.37 – 8.36 (m, 1H), 7.18

– 6.91 (m, 7H), 4.27*/4.22 (d, *J* = 5.4 Hz, 2H), 4.05*/3.82 (s, 2H), 3.59/3.56* (s, 3H), 3.36 – 3.16

(m, 2H), 2.33 – 2.18 (m, 11H), 1.56 – 1.05 (m, 6H). ^{13}C NMR (126 MHz, DMSO-d_6) δ 173.3,

173.2, 171.1, 168.10, 168.07, 137.44, 137.41, 136.7, 136.5, 136.4, 136.2, 135.9, 135.8, 130.5,

128.8, 127.3, 127.2, 124.0, 51.4, 51.17, 51.15, 49.5, 47.5, 45.6, 41.9, 41.8, 33.2, 33.0, 27.3, 26.1,

25.8, 25.3, 24.2, 23.8, 20.8, 20.7. Anal. Calcd. for $C_{26}H_{34}N_2O_4$: C 71.21, H 7.81, N 6.39. Found:

C 71.28, H 8.00, N 6.19.

Methyl 6-(*N*-{2-[(3,5-dimethylbenzyl)amino]-2-oxoethyl}-3,5-dimethylbenzamido)hexa-

noate (10b). White solid; 52%; mp. 83 °C; ^{1}H NMR (600 MHz, DMSO-d_6) δ 8.35 – 8.34 (m, 1H),

7.06 – 6.81 (m, 6H), 4.25*/4.19 (d, *J* = 5.4 Hz, 2H), 4.06*/3.83 (s, 2H), 3.59/3.55* (s, 3H), 3.36 –

3.16 (m, 2H), 2.33 – 2.18 (m, 14H), 1.56 – 1.05 (m, 6H). ^{13}C NMR (126 MHz, DMSO-d_6) δ 173.3,

173.2, 171.1, 168.1, 139.2, 138.9, 137.5, 137.4, 137.23, 137.16, 136.7, 136.5, 130.5, 128.3, 128.1,

125.2, 125.0, 124.0, 51.4, 51.2, 51.1, 49.5, 47.5, 45.6, 42.2, 42.0, 33.2, 33.0, 27.3, 26.1, 26.0, 25.3,

24.2, 23.8, 20.9, 20.7. Anal. Calcd. for $C_{27}H_{36}N_2O_4$: C 71.65, H 8.02, N 6.19. Found: C 71.49,

H 8.11, N 6.11.

***tert*-Butyl {2-[6-(3,5-dimethyl-*N*-{2-[(4-methylbenzyl)amino]-2-oxoethyl}benzamido)-he-**

xanamido]phenyl}carbamate (11a). White solid; 60%; mp. 78 °C; ^{1}H NMR (600 MHz, DMSO-

d_6) δ 9.45/9.38* (s, 1H), 8.37 – 8.30 (m, 2H), 7.54 – 6.92 (m, 11H), 4.28*/4.22 (d, *J* = 5.3 Hz, 2H),

4.06*/3.83 (s, 2H), 3.40 – 3.19 (m, 2H), 2.38 – 2.21 (m, 11H), 1.64 – 1.12 (m, 15H). ^{13}C NMR

(151 MHz, DMSO-d_6) δ 171.7, 171.5, 171.11, 171.08, 168.09, 168.05, 153.1, 153.0, 137.44,

137.40, 136.7, 136.5, 136.4, 136.2, 135.9, 135.8, 131.1, 131.0, 130.47, 130.46, 129.7, 129.6, 128.8,

127.3, 127.2, 125.0, 124.8, 124.0, 123.8, 123.6, 79.33, 79.30, 51.4, 49.7, 47.5, 45.8, 41.92, 41.85,

35.9, 35.8, 28.1, 27.6, 26.3, 26.0, 25.5, 25.0, 24.7, 20.8, 20.6. HRMS (ESI) [M+H]$^+$: 615.3547,

Calcd. for $C_{36}H_{47}N_4O_5$: 615.3541. Anal. Calcd. for $C_{36}H_{46}N_4O_5$: C 70.33, H 7.54, N 9.11. Found:

C 70.08, H 7.63, N 8.83.

tert-Butyl {2-[6-(N-{2-[(3,5-dimethylbenzyl)amino]-2-oxoethyl}-3,5-dimethylbenzamido)-hexanamido]phenyl}carbamate (11b). White solid; 59%; mp. 75 °C; t_R = 18.92 min, 98.2%

purity; ^{1}H NMR (600 MHz, DMSO-d_6) δ 9.44/9.38* (s, 1H), 8.36 – 8.30 (m, 2H), 7.53 – 6.81 (m,

10H), 4.25*/4.19 (d, J = 4.9 Hz, 1H), 4.07*/3.84 (s, 2H), 3.39 – 3.21 (m, 2H), 2.37 – 2.21 (m, 14H),

1.64 – 1.13 (m, 15H). ^{13}C NMR (151 MHz, DMSO-d_6) δ 171.7, 171.5, 171.10, 171.07, 168.1,

153.1, 153.0, 139.2, 138.9, 137.44, 137.37, 137.22, 137.16, 136.7, 136.5, 131.1, 130.48, 130.46,

129.6, 128.3, 128.1, 125.2, 125.0, 124.8, 124.0, 123.8, 123.6, 79.33, 79.31, 51.4, 49.7, 47.5, 45.7,

42.2, 42.0, 35.9, 35.8, 28.0, 27.6, 26.3, 26.0, 25.5, 25.0, 24.7, 21.0, 20.8, 20.7. HRMS (ESI)

[M+H]$^+$: 629.3697, Calcd. for $C_{37}H_{49}N_4O_5$: 629.3697.

Methyl 4-({N-[2-(benzylamino)-2-oxoethyl]-4-(dimethylamino)benzamido}methyl)-ben-zoate (12a). White solid; 68%; mp. 131 °C; ^{1}H NMR (600 MHz, DMSO-d_6) δ 8.49 – 8.41 (m,

1H), 7.96 – 6.64 (m, 13H), 4.71 (bs, 2H), 4.30 (d, J = 5.8 Hz), 3.92 (bs, 2H), 3.85 (s, 3H), 2.93 (s,

6H). ^{13}C NMR (151 MHz, DMSO-d_6) δ 171.8, 168.1, 166.1, 151.2, 143.3, 139.2, 129.4, 128.6,

128.5, 128.3, 128.0, 127.3, 126.8, 122.0, 110.9, 52.1, 51.5, 49.3, 42.1, 39.7. Anal. Calcd. for

$C_{27}H_{29}N_3O_4$: C 70.57; H 6.36; N 9.14. Found: C 70.44; H 6.45; N 9.04.

Methyl 4-({N-[2-(benzylamino)-2-oxoethyl]-3,5-dimethylbenzamido}methyl)benzoate (12b).

White solid; 73%; mp. 82 °C; ^{1}H NMR (600 MHz, DMSO-d_6) δ 8.45*/8.40 (t, J = 5.7 Hz, 1H),

7.97 – 7.01 (m, 1H), 4.73/4.60* (s, 2H), 4.33*/4.28 (d, J = 5.8 Hz, 2H), 4.02*/3.82 (s, 2H), 3.86 (s,

3H) 2.26/2.24* (s, 6H). ^{13}C NMR (151 MHz, DMSO-d_6) δ 171.6, 167.8, 167.6, 166.1, 166.0, 143.0, 142.8, 139.3, 139.1, 137.6, 135.9, 135.8, 130.1, 129.5, 129.4, 128.7, 128.5, 128.30, 128.26, 127.9, 127.24, 127.16, 126.9, 126.8, 124.1, 53.3, 52.1, 51.2, 48.8, 47.7, 42.2, 42.1, 20.8. Anal. Calcd. for $C_{27}H_{28}N_2O_4$: C 72.95; H 6.35; N 6.30. Found: C 72.97; H 6.35; N 6.21.

Methyl 4-({*N*-[2-(benzylamino)-2-oxoethyl]nicotinamido}methyl)benzoate (12c). White solid; 78%; mp. 105 °C; ^{1}H NMR (600 MHz, DMSO-d_6) δ 8.69 − 7.12 (m, 14H), 4.74/4.64* (s, 2H), 4.34*/4.24 (d, *J* = 5.7 Hz, 2H), 4.09*/3.89 (s, 2H), 3.86 (s, 3H). ^{13}C NMR (151 MHz, DMSO-d_6) δ 169.6, 169.4, 167.6, 167.4, 166.1, 166.0, 150.6, 150.5, 147.4, 147.0, 142.6, 142.4, 139.2, 138.8, 134.5, 134.4, 131.9, 131.6, 129.6, 129.4, 128.8, 128.6, 128.3, 128.0, 127.2, 126.9, 126.8, 123.6, 123.4, 53.4, 52.1, 51.4, 49.2, 48.3, 42.3, 42.1. Anal. Calcd. for $C_{24}H_{23}N_3O_4$: C 69.05, H 5.55, N 10.07. Found: C 68.84, H 5.72, N 9.76.

***tert*-Butyl {2-[4-({*N*-[2-(benzylamino)-2-oxoethyl]-4-(dimethylamino)benzamido}methyl)-benzamido]phenyl}carbamate (13a).** White solid; 61%; mp. 126 °C; ^{1}H NMR (500 MHz, DMSO-d_6) δ 9.82 (s, 1H), 8.64 (s, 1H), 8.43 (t, *J* = 5.3 Hz, 1H), 7.96 − 6.65 (m, 17H), 4.73 (s, 2H), 4.32 (d, *J* = 5.8 Hz, 2H), 3.93 (s, 2H), 2.94 (s, 6H), 1.45(s, 9H). ^{13}C NMR (126 MHz, DMSO-d_6) δ 171.7, 168.1, 165.0, 153.4, 151.2, 141.6, 139.2, 133.1, 131.7, 129.7, 128.5, 128.2, 127.8, 127.2, 126.8, 125.9, 125.5, 124.0, 123.8, 110.9, 79.6, 42.1, 28.0. HRMS (ESI) [M+H]$^+$: 636.3182, Calcd. for $C_{37}H_{42}N_5O_5$: 636.3180. Anal. Calcd. for $C_{37}H_{41}N_5O_5$: C 69.90; H 6.50; N 11.02. Found: C 69.63; H 6.63; N 10.90.

tert-Butyl {2-[4-({*N*-[2-(benzylamino)-2-oxoethyl]-3,5-dimethylbenzamido}methyl)benz-amido]phenyl}carbamate (13b). White solid; 62%; mp. 122 °C; ^{1}H NMR (500 MHz, DMSO-d_6) δ 9.84 (s, 1H), 8.68 (s, 1H), 8.46*/8.41 (t, *J* = 5.8 Hz, 1H), 7.97– 7.03 (m, 16H), 4.74/4.61* (s, 2H), 4.34*/4.29 (d, *J* = 5.8 Hz, 2H), 4.02*/3.82 (s, 2H), 2.25 (s, 6H), 1.45 (s, 9H). ^{13}C NMR (126 MHz, DMSO-d_6) δ 171.63, 171.60, 167.8, 167.6, 165.1, 165.0, 153.5, 141.4, 141.1, 139.3, 139.1, 137.6, 136.0, 135.9, 133.3, 133.2, 131.8, 131.7, 130.9, 130.8, 129.7, 128.31, 128.27, 128.0, 127.9, 127.8, 127.3, 127.2, 127.0, 126.9, 126.8, 126.1, 126.0, 125.6, 124.11, 124.08, 123.9, 79.7, 53.2, 51.1, 48.7, 47.5, 42.2, 42.1, 28.0, 20.8. HRMS (ESI) [M+H]$^{+}$: 621.3067, Calcd. for $C_{37}H_{41}N_4O_5$: 621.3071. Anal. Calcd. for $C_{37}H_{40}N_4O_5$: C 71.59; H 6.50; N 9.03. Found: C 71.16; H 6.71; N 8.76.

tert-Butyl {2-[4-({*N*-[2-(benzylamino)-2-oxoethyl]nicotinamido}methyl)benzamido]phe-nyl}carbamate (13c). White solid; 25%; mp. 115 °C; t_R = 13.48 min, 96.1% purity; ^{1}H NMR (600 MHz, DMSO-d_6) δ 9.85 (s, 1H), 8.69 – 8.13 (m, 19H), 4.76/4.66* (s, 2H), 4.35*/4.25 (d, *J* = 5.4 Hz, 2H), 4.09*/3.89 (s, 2H), 1.44 (s, 9H). ^{13}C NMR (151 MHz, DMSO-d_6) δ 169.5, 169.3, 167.6, 167.4, 165.1, 165.0, 153.4, 150.7, 150.5, 147.4, 147.1, 141.0, 140.7, 139.3, 138.8, 134.5, 134.4, 133.4, 133.2, 132.0, 131.8, 129.7, 128.3, 128.1, 127.9, 127.8, 127.23, 127.16, 126.9, 126.8, 126.1, 125.6, 124.1, 123.8, 123.6, 123.4, 79.7, 53.4, 51.3, 49.1, 48.2, 42.3, 42.1, 28.0. HRMS (ESI) [M+H]$^{+}$: 594.2708, Calcd. for $C_{34}H_{36}N_5O_5$: 594.2711.

tert-Butyl {3-[4-({*N*-[2-(benzylamino)-2-oxoethyl]-3,5-dimethylbenzamido}methyl)benz-amido]-[1,1'-biphenyl]-4-yl}carbamate (13d). White solid; 65%; mp. 199 °C; t_R = 20.30 min, 98.0 purity; ^{1}H NMR (600 MHz, DMSO-d_6) δ 9.93 (s, 1H), 8.78 (s, 1H), 8.46*/8.42 (t, *J* = 5.6 Hz, 1H), 7.99 – 7.03 (m, 20H), 4.75/4.62* (s, 2H), 4.34*/4.29 (d, *J* = 5.6 Hz, 2H), 4.02*/3.82 (s, 2H),

2.25 (s, 6H), 1.47 (s, 9H). ^{13}C NMR (151 MHz, DMSO-d_6) δ 171.62, 171.61, 167.8, 167.7, 165.3, 165.1, 153.4, 141.4, 141.1, 139.3, 139.1, 137.6, 136.0, 135.9, 133.3, 133.2, 131.20, 131.15, 130.9, 130.8, 129.9, 129.0, 128.31, 128.27, 128.1, 127.9, 127.8, 127.4, 127.3, 127.2, 127.0, 126.9, 126.8, 126.4, 124.12, 124.08, 123.8, 79.8, 53.2, 51.1, 48.7, 47.6, 42.2, 42.1, 28.0, 20.8. HRMS (ESI) [M+H]$^+$: 697.3380, Calcd. for C$_{43}$H$_{45}$N$_4$O$_5$: 697.3384.

tert-Butyl {3-[4-({*N*-[2-(benzylamino)-2-oxoethyl]-4-(dimethylamino)benzamido}methyl)-benzamido]-[1,1'-biphenyl]-4-yl}carbamate (13e). Rose solid; 65%; mp. 203 °C; ^{1}H NMR (600 MHz, DMSO-d_6) δ 9.93 (s, 1H), 8.77 (s, 1H), 8.52 – 8.43 (m, 1H), 7.99 – 6.66 (m, 21H), 4.74 (bs, 2H), 4.32 (d, *J* = 5.8 Hz, 2H), 3.93 (bs, 2H), 2.94 (s, 6H), 1.47 (s, 9H,). ^{13}C NMR (151 MHz, DMSO-d_6) δ 171.8, 168.2, 165.3, 153.4, 151.3, 141.7, 139.3, 135.8, 133.1, 131.2, 129.9, 129.0, 128.6, 128.3, 128.0, 127.9, 127.4, 127.3, 126.9, 126.4, 124.12, 124.05, 123.8, 111.0, 79.8, 42.1, 28.1. HRMS (ESI) [M+H]$^+$: 712.3490, Calcd. for C$_{43}$H$_{46}$N$_5$O$_5$: 712.3493. Anal. Calcd. for C$_{43}$H$_{45}$N$_5$O$_5$: C 72.55, H 6.37, N 9.84. Found: C 72.28, H 6.40, N 9.71.

tert-Butyl {2-[4-({*N*-[2-(benzylamino)-2-oxoethyl]-3,5-dimethylbenzamido}methyl)benz-amido]-4-fluorophenyl}carbamate (13f). White solid; 65%; mp. 191 °C; ^{1}H NMR (600 MHz, DMSO-d_6) δ 9.82 (s, 1H), 8.79 (bs, 1H), 8.46*/8.41 (t, *J* = 5.7 Hz, 1H), 7.95 – 7.03 (m, 15H), 4.74/4.61* (s, 2H), 4.33*/4.28 (d, *J* = 5.6 Hz, 2H), 4.01*/3.81 (s, 2H), 2.25 (s, 6H, 2 x CH$_3$), 1.45 (s, 9H). ^{13}C NMR (151 MHz, DMSO-d_6) δ 171.6, 167.8, 167.6, 165.1, 164.9, 159.2, 157.6, 153.7, 141.6, 141.3, 139.3, 139.1, 137.6, 136.0, 135.8, 133.1, 133.0, 131.8, 131.8, 130.9, 130.9, 128.31, 128.27, 128.0, 127.9, 127.34, 127.25, 127.2, 127.1, 126.9, 126.8, 125.9, 124.1, 112.0, 111.9, 111.8, 111.7, 111.6, 79.7, 53.2, 51.1, 48.7, 47.6, 42.2, 42.1, 28.0, 20.8. HRMS (ESI) [M+H]$^+$: 639.2979,

Calcd. for $C_{37}H_{40}FN_4O_5$: 639.2977. Anal. Calcd. for $C_{37}H_{39}FN_4O_5$: C 69.58, H 6.15, N 8.77. Found: C 69.81, H 6.21, N 8.78.

Biological evaluation

Reagents. Cisplatin was purchased from Sigma (Germany) and dissolved in 0.9% sodium chloride solution, propidium iodide (PI) was purchased from PromoKine (Germany). Vorinostat was synthesized according to known procedures.[30] Stock solutions (10 mM) of **1h**, **2a**, **2d**, entinostat, nexturastat A, and vorinostat were prepared with DMSO and diluted to the desired concentrations with the appropriate medium. All other reagents were supplied by PAN Biotech (Germany) unless otherwise stated.

Cell lines and cell culture. The human ovarian carcinoma cell line A2780 was obtained from European Collection of Cell Cultures (ECACC, UK). The human tongue cell line Cal27 was obtained from the German Collection of Microorganisms and Cell Cultures (DSMZ, Germany). The corresponding cisplatin resistant CisR cell line Cal27CisR was

generated by exposing the parental cell line to weekly cycles of cisplatin in an IC_{50}

concentration over a period of 24 - 30 weeks as described in Gosepath *et al.* and

Eckstein *et al.* [15, 31] All cell lines were grown at 37°C under humidified air

supplemented with 5% CO_2 in RPMI 1640 (A2780) or DMEM (Cal27) containing 10%

fetal calf serum, 120 IU/mL penicillin, and 120 µg/mL streptomycin. The cells were

grown to 80% confluency before being used in further assays.

MTT cell viability assay. The rate of cell-survival under the action of test substances

was evaluated by an improved MTT assay as previously described.[32,33] A2780 and

Cal27 cell lines were seeded at a density of 5,000 and 2,500 cells/well in 96 well plates

(Corning, Germany). After 24 h, cells were exposed to increased concentrations of the

test compounds. Incubation was ended after 72 h and cell survival was determined by

addition of MTT (Serva, Germany) solution (5 mg/mL in phosphate buffered saline).

The formazan precipitate was dissolved in DMSO (VWR, Germany). Absorbance was

measured at 544 nm and 690 nm in a FLUOstar microplate-reader (BMG LabTech,

Germany). To investigate the effect of **1h**, **2a**, and **2d** on cisplatin induced cytotoxicity,

compounds were added 48 h before cisplatin administration. After 72 h, the cytotoxic

effect was determined by MTT assay as described above, and shift factors were

calculated by dividing the IC_{50} value of cisplatin alone by the IC_{50} value of the drug

combinations.

Combination index analysis. The combined effect of cisplatin and **1h**, **2a**, or **2d** was

analyzed using the MTT assay. Cell viability was determined from each well relative to

the average absorbance of control wells. The combination indexes (CIs) were calculated

with the CalcuSyn 2.1 software (BioSoft, Cambridge) based on the Chou-Talalay method.

A CI > 1 indicates antagonism, a CI = 1 indicates an additive effect, and a CI < 1 indicates

synergism.

Whole-cell HDAC inhibition assay. The cellular HDAC assay was based on an assay

published by Ciossek *et al*.[34] and Bonfils *et al*.[35] with minor modifications as described

in Marek *et al*..[32]

Briefly, human cancer cell lines Cal27 and A2780 were seeded in 96-well tissue culture

plates (Corning, Germany) at a density of 1.5 x 10^4 cells/well in a total volume of 90

µL culture medium. After 24 h, cells were incubated for 18 h with increasing

concentrations of test compounds. The reaction was started by adding 10 µL of 3 mM

Boc-Lys(ε-Ac)-AMC (Bachem, Germany) to reach a final concentration of 0.3 mM.[36]

Cells were incubated with Boc-Lys(ε-Ac)-AMC for 3 h under cell culture conditions.

Then, 100 µl/well stop solution (25 mM Tris-HCl (pH 8), 137 mM NaCl, 2.7 mM KCl, 1

mM $MgCl_2$, 1% NP40, 2.0 mg/mL trypsin, 10 µM vorinostat) was added and the

reaction was developed for 3 h under cell culture conditions. Fluorescence intensity

was measured at an excitation of 320 nm and emission of 520 nm in a NOVOstar

microplate-reader (BMG LabTech, Offenburg, Germany).

Measurement of apoptotic nuclei. Cal27 and Cal27CisR cells were seeded at a density

of 3 x 10^4 cells/well in 24-well plates (Sarstedt, Germany). Cells were treated with **1h**, **2a**,

or **2d** and cisplatin alone or in combination for the indicated time points. Supernatant was

removed after a centrifugation step and the cells were lysed in 500 µL hypotonic lysis

buffer (0.1% sodium citrate, 0.1% Triton X-100, 100 µg/mL PI) at 4°C in the dark

overnight. The percentage of apoptotic nuclei with DNA content in sub-G1 was analyzed

by flow cytometry using the CyFlow instrument (Partec, Germany).

Caspase 3/7 activation assay. Compound-induced activation of caspases 3 and 7 was

analyzed using the CellEvent Caspase-3/7 green detection reagent (Thermo Scientific,

Germany) according to the manufacturer´s instructions. Briefly, Cal27 and Cal27CisR

cells were seeded in 96-well-plates (Corning, Germany) at a density of 900 cells/ well.

Cells were treated with **1h**, **2a**, or **2d** 48h prior to the addition cisplatin and another

incubation period of 24h. Then, medium was removed and 50 µL of CellEvent Caspase

3/7 green detection reagent (2 µM in PBS supplemented with 5% heat inactivated FBS)

were added. Cells were incubated for 30 min at 37°C in a humidified incubator before

imaging by using the Thermo Fisher ArrayScan XTI high content screening (HCS) system

(Thermo Scientific). Hoechst 33342 was used for nuclear staining. The pan caspase

inhibitor QVD was used in a concentration of 20 µM diluted in the appropriate medium

and incubated 30 minutes prior to compound addition.

Immunoblotting. Cells were treated with 5 µM of **1h**, 0.5 µM **2a**, 3.2 µM **2d**, or vehicle

for 24 h. The HDACi entinostat, nexturastat A, and vorinostat were used as controls.

Cell pellets were dissolved with RIPA buffer (50 mM Tris-HCl pH8.0, 1% Triton X-100,

0.5% sodium deoxycholate, 0.1% SDS, 150 mM sodium chloride, 2 mM EDTA,

supplemented with protease and phosphatase inhibitors (Pierce™ protease and

phosphatase inhibitor mini tablets, Thermo Scientific)) and clarified by centrifugation.

Equal amounts of total protein (20 µg) were resolved by SDS-PAGE and transferred

to polyvinylidene fluoride membranes (Merck Millipore). Blots were incubated with

primary antibodies against acetylated α-tubulin, α-tubulin (Santa Cruz Biotechnology,

Germany), and acetyl histone H3 (Lys24) (biotechne, Germany). Immunoreactive

proteins were visualized using luminol reagent (Santa Cruz Biotechnology, Germany)

with an Intas Imager (Intas, Germany). Densitometric analysis was performed on

scanned images using the Image J software (National Institute of Health).[37]

Data Analysis. Concentration-effect curves were constructed with Prism 7.0 (GraphPad, San Diego, CA) by fitting the pooled data of at least three experiments performed in triplicates to the four parameter logistic equation. Statistical analysis was performed using t test or one-way ANOVA.

In-vitro **HDAC1 and HDAC6 assay.** OptiPlate-96 black microplates (Perkin Elmer) were used with an assay volume of 50 µL. Human recombinant HDAC1 (10 ng/well; BPS Bioscience, Catalog #: 50051) or HDAC6 (35 ng/well; BPS Bioscience, Catalog #: 50006) were diluted in assay buffer (50 mM Tris–HCl, pH 8.0, 137 mM NaCl, 2.7 mM KCl, 1 mM $MgCl_2$, 0.1 mg/mL BSA), followed by addition of different concentrations of test compounds or controls diluted in assay buffer and 5 µL of the fluorogenic substrate ZMAL (Z-(Ac)Lys-AMC)[38] (150 µM) at 37 °C. After 90 min incubation at 37 °C, 50 µL of 0.4 mg/mL trypsin in trypsin buffer (Tris–HCl 50 mM, pH 8.0, NaCl 100 mM)) was added, followed by further incubation at 37 °C for 30 min. Fluorescence was measured with an

excitation wavelength of 390 nm and an emission wavelength of 460 nm using a Spark

10 M microplate reader (Tecan).

In-vitro HDAC2 and HDAC3 assay. Black 96-well flat bottom microplates (Corning®

Costar®, Corning Incorporated, NY) were used. Human recombinant C-terminal FLAG-

tag HDAC2 (BPS Bioscience, Catalog #: 50052) or human recombinant C-terminal His-

tag HDAC3/NcoR2 (BPS Bioscience, Catalog #: 50003) were diluted in incubation buffer

(25 mM Tris-HCl, pH 8.0, 137 mM NaCl, 2.7 mM KCl, 1 mM MgCl, 0.01% Triton-X and 1

mg/mL BSA). 40 µL of this dilution was incubated with 10 µL of different concentrations

of inhibitors in 10% DMSO/incubation buffer and 50 µL of the fluorogenic Boc-Lys(ε-Ac)-

AMC (20 µM, Bachem, Germany) at 37 °C. After 90 min incubation time 50 µL of the stop

solution (25 mM Tris-HCl (pH 8), 137 mM NaCl, 2.7 mM KCl, 1 mM MgCl2, 0.01% Triton-

X, 6.0 mg/mL trypsin from porcine pancreas Type IX-S, lyophilized powder, 13,000-

20,000 BAEE units/mg protein (Sigma Aldrich) and 200 µM vorinostat) was added. After

a following incubation at 37 °C for 30 min, the fluorescence was measured on a Synergy

H1 Hybrid Multi-Mode Microplate Reader (BioTek, USA) with a gain of 70 and an

excitation wavelength of 370 nm and an emission wavelength of 460 nm.

In-vitro **HDAC4 and HDAC8 assay.** All human recombinant enzymes were purchased from Reaction Biology Corp. (Malvern, PA, USA). The HDAC activity assay of HDAC4 (catalog nr. KDA-21-279) and HDAC8 (catalog nr. KDA-21-481) was performed in 96-well plates (Corning, Germany). Briefly, 20 ng of HDAC8 and 2 ng of HDAC4 per reaction were used. Recombinant enzymes were diluted in assay buffer (50 mM Tris-HCl, pH 8.0, 137 mM NaCl, 2.7 mM KCl, 1 mM $MgCl_2$, and 1 mg/ml BSA). 80 µl of this dilution was incubated with 10 µl of different concentrations of inhibitors in assay buffer. After a 5 min incubation step, the reaction was started with 10 µl of 100 µM (HDAC4) or 60 µM (HDAC8) Boc-Lys(TFa)-AMC (Bachem, Germany). The reaction was stopped after 90 min by adding 100 µl stop solution (16mg/ml trypsin, 2 µM panobinostat for HDAC8, 2 µM or CHDI0039 (kindly provided by the CHDI Foundation Inc., New York, USA) for HDAC4 in 50 mM Tris-HCl, pH 8.0, and 100 mM NaCl. 15 min after the addition of the stop solution, fluorescence intensity was measured at excitation of 355 nm and emission of 460 nm in a NOVOstar microplate reader (BMG LabTech, Offenburg, Germany).

Docking studies

We docked the *cis*- and *trans*-rotamers of compounds **1f**, **1h**, and **2a** into X-ray crystal

structures of HDACs 1 (PDB ID: 4BKX)[39], 2 (PDB ID: 4LY1)[40], 3 (PDB ID: 4A69)[41], and 6

(PDB ID: 5EDU)[42] to understand and explain their selectivity profiles. All HDAC crystal

structures were energy minimized with Moloc using the MAB force field.[43] The compounds

were drawn with ChemDraw Ultra, converted into a 3D structure, and energy minimized

with Moloc using the MAB force field.[43] The HDACi's were then docked into the HDAC

structures utilizing AutoDock3[44] as a docking engine and the DrugScore[45,46] distance-

dependent pair-potentials as an objective function, as described in ref[47]. In the docking,

default parameters were used with the exception of the clustering RMSD cutoff, which

was set to 2.0 Å, to consider the flexibly connected saturated and unsaturated carbon

cycles. Docking solutions with more than 20% of all configurations in the largest cluster

were considered sufficiently converged. The configuration in the largest cluster with the

lowest docking energy and with a distance < 3 Å between the hydroxamic acid oxygen

and the zinc ion in the binding pocket was used for further evaluation.

PAINS Analysis

We filtered all compounds for pan-assay interference compounds (PAINS) using the

online filter http://zinc15.docking.org/patterns/home/.[48] No compound was flagged as

PAINS.

ASSOCIATED CONTENT

Supporting Information.

The Supporting Information is available free of charge on the ACS Publications website

at DOI: 10.1021/acs.jmedchem.xxxxx.

Supplementary Table and Figures, ^{1}H and ^{13}C NMR spectra, and HPLC chromatograms

(PDF)

Coordinate information of docked complexes (PDB)

Molecular formula strings and some data (CSV)

Notes

PDB IDs 4BKX (HDAC1), 4LY1 (HDAC2), 4A69 (HDAC3), 5EDU (HDAC6) were used for

docking *cis*- and *trans*-rotamers of compounds **1f**, **1h**, and **2a**.

AUTHOR INFORMATION

Corresponding Authors

* Phone: (+49) 341 97 36801, Fax (+49) 341 97 36889, E-mail:

finn.hansen@medizin.uni-leipzig.de; Phone: +49 211 81-14587, , Email:

matthias.kassack@uni-duesseldorf.de.

Author Contributions

#These authors contributed equally to this work.

‡These authors share the senior authorship.

ACKNOWLEDGMENT

ABBREVIATIONS

CisR, cisplatin resistant subclone; DIC, diisopropylcarbodiimide; EDC·HCl, *N*-(3-Dimethylaminopropyl)-*N*-ethylcarbodiimide hydrochloride; DMAP, 4-(dimethylamino)pyridine; Et$_3$N, triethylamine; HAT, histone acetyltransferase; HDAC, histone deacetylase; HDACi, histone deacetylase inhibitor; HOAt, 1-Hydroxy-7-azabenzotriazol; MTT, 3-(4,5-dimethylthiazol-2-yl)-2,5-diphenyltetra-zolium bromide; MS, molecular sieves; RT, room temperature; U-4CR, ugi 4-component reaction; ZBG, zinc-binding group.

REFERENCES

(1) (a) Wagner, J. M.; Hackanson, B.; Lübbert, M.; Jung, M. Histone deacetylase (HDAC) inhibitors in recent clinical trials for cancer therapy. *Clin. Epigenet.* **2010**, *1*, 117–136. (b) Witt, O.; Deubzer, H. E.; Milde, T.; Oehme, I. HDAC family: what are the cancer relevant targets? *Cancer Lett.* **2009**, *277*, 8–21. (c) Biel, M.; Wascholowski, V.; Giannis, A. Epigenetics - an epicenter of gene regulation: histones and histone-modifying enzymes. *Angew. Chem. Int. Ed.* **2005**, *44*, 3186–3216.

(2) New, M.; Olzscha, H.; La Thangue, N. B. HDAC inhibitor-based therapies: can we interpret the code? *Mol. Oncol.* **2012**, *6*, 637–656.

(3) Mottamal, M.; Zheng, S.; Huang, T. L.; Wang, G. Histone deacetylase inhibitors in clinical studies as templates for new anticancer agents. *Molecules* **2015**, *20*, 3898–3941.

(4) (a) Paris, M.; Porcelloni, M.; Binaschi, M.; Fattori, D. Histone deacetylase inhibitors: from bench to clinic. *J. Med. Chem.* **2008**, *51*, 1505–1529. (b) Andrews, K. T.; Haque, A.; Jones, M. K. HDAC inhibitors in parasitic diseases. *Immunol. Cell Biol.* **2012**, *90*, 66–77. (c) Xiao, H.; Jiao, J.; Wang, L.; O'Brien, S.; Newick, K.; Wang, L.-C.

S.; Falkensammer, E.; Liu, Y.; Han, R.; Kapoor, V.; Hansen, F. K.; Kurz, T.; Hancock, W. W.; Beier, U. H. HDAC5 controls the functions of Foxp3^{+} T-regulatory and CD8^{+} T cells. *Int. J. Cancer* **2016**, *138*, 2477–2486. (d) Archin, N. M.; Liberty, A. L.; Kashuba, A. D.; Choudhary, S. K.; Kuruc, J. D.; Crooks, A. M.; Parker, D. C.; Anderson, E. M.; Kearney, M. F.; Strain, M. C.; Richman, D. D.; Hudgens, M. G.; Bosch, R. J.; J.M.Coffin, J. M.; Eron, J. J.; Hazuda, D. J.; Margolis, D. M. Administration of vorinostat disrupts HIV-1 latency in patients on antiretroviral therapy. *Nature* **2012**, *487*, 482–485. (e) Cao, F.; Zwinderman, M. R. H.; Dekker, F. J. The process and strategy for developing selective histone deacetylase 3 inhibitors. *Molecules* **2018**, *23*, 551. (f) Trazzi, S.; Fuchs, C.; Viggiano, R.; de Franceschi, M.; Valli, E.; Jedynak, P.; Hansen, F. K.; Perini, G.; Rimondini, R.; Kurz, T.; Bartesaghi, R.; Ciani, E. HDAC4: a key factor underlying brain developmental alterations in CDKL5 disorder. *Hum. Mol. Genet.* **2016**, *25*, 3887–3907. (g) Falkenberg, K. J.; Johnstone, R. W. Histone deacetylases and their inhibitors in cancer, neurological diseases and immune disorders. *Nat. Rev. Drug Discov.* **2014**, *13*, 673–691.

(5) Whittle, J. R.; Desai, J. Histone deacetylase inhibitors in cancer: what have we learned? *Cancer* **2015**, *121*, 1164–1167.

(6) Shen, S.; Kozikowski, A. P. Why hydroxamates may not be the best histone deacetylase inhibitors-what some may have forgotten or would rather forget? *ChemMedChem* **2016**, *11*, 15-21.

(7) Bressi, J. C.; Jennings, A. J.; Skene, R.; Wu, Y.; Melkus, R.; De Jong, R.; O'Connell, S.; Grimshaw, C. E.; Navre, M.; Gangloff, A. R. Exploration of the HDAC2 foot pocket: synthesis and SAR of substituted N-(2-aminophenyl)benzamides. *Bioorg. Med. Chem. Lett.* **2010**, *20*, 3142–3145.

(8) (a) Shi, Y.; Dong, M.; Hong, X.; Zhang, W.; Feng, J.; Zhu, J.; Yu, L.; Ke, X.; Huang, H.; Shen, Z.; Fan, Y.; Li, W.; Zhao, X.; Qi, J.; Zhou, D.; Ning, Z.; Lu, X. Results from a multicenter, open-label, pivotal phase II study of chidamide in relapsed or refractory peripheral T-cell lymphoma. *Ann. Oncol.* **2015**, 1766–1771. (b) Pan, D.-S.; Yang, Q.-J.; Fu, X.; Shan, S.; Zhu, J.-Z.; Zhang, K.; Li, Z.-B.; Ning, Z.-Q.; Lu, X.-P. Discovery of an orally active subtype-selective HDAC inhibitor, chidamide, as an epigenetic modulator for cancer treatment. *Med. Chem. Commun.* **2014**, *5*, 1789–1796.

(9) (a) Roche, J.; Bertrand, P. Inside HDACs with more selective HDAC inhibitors. *Eur. J. Med. Chem.* **2016**, *121*, 451–483. (b) Rai M.; Soragni E.; Chou C.J.; Barnes G.; Jones S.; Rusche J.R.; Gottesfeld J.M.; Pandolfo M.; Two new pimelic diphenylamide HDAC inhibitors induce sustained frataxin upregulation in cells from Friedreich's ataxia patients and in a mouse model. *PLoS One.* **2010**, *5*; e8825.

(10)   (a) Diedrich, D.; Hamacher, A.; Gertzen, C. G. W.; Alves Avelar, L. A.; Reiss, G. J.; Kurz, T.; Gohlke, H.; Kassack, M. U.; Hansen, F. K. Rational design and diversity-oriented synthesis of peptoid-based selective HDAC6 inhibitors. *Chem. Commun.* **2016**, *52*, 3219–3222. (b) Porter, N. J.; Osko, J. D.; Diedrich, D.; Kurz, T.; Hooker, J. M.; Hansen, F. K.; Christianson, D. W. Histone deacetylase 6-selective inhibitors and the influence of capping groups on hydroxamate-zinc denticity. *J. Med. Chem.* **2018**, *61*, 8054–8060. (c) Diedrich, D.; Stenzel, K.; Hesping, E.; Antonova-Koch, Y.; Gebru, T.; Duffy, S.; Fisher, G.; Schöler, A.; Meister, S.; Kurz, T.; Avery, V. M.; Winzeler, E. A.; Held, J.; Andrews, K. T.; Hansen, F. K. One-pot, multi-component synthesis and structure-activity relationships of peptoid-based histone deacetylase (HDAC) inhibitors targeting malaria parasites. *Eur. J. Med. Chem.* **2018**, *158*, 801–813.

(11)   Krieger, V.; Hamacher, A.; Gertzen, C. G. W.; Senger, J.; Zwinderman, M. R. H.;

Marek, M.; Romier, C.; Dekker, F. J.; Kurz, T.; Jung, M.; Gohlke, H.; Kassack, M. U.;

Hansen, F. K. Design, multicomponent synthesis, and anticancer activity of a focused

histone deacetylase (HDAC) inhibitor library with peptoid-based cap groups. *J. Med.

Chem.* **2017**, *60*, 5493–5506.

(12)   Kim, R.; Skolnick, J. Assessment of programs for ligand binding affinity prediction.

J. Comput. Chem. **2008**, *29*, 1316–1331.

(13)   Jurkin, J.; Zupkovitz, G.; Lagger, S.; Grausenburger, R.; Hagelkruys, A.; Kenner,

L.; Seiser, C. Distinct and redundant functions of histone deacetylases HDAC1 and

HDAC2 in proliferation and tumorigenesis. *Cell Cycle* **2011**, *10(3)*, 406-412

(14)   Bradner, J. E.; Hnisz, D.; Young, R. A. Transcriptional addiction in cancer. *Cell*

2016, *168*, 629–643.

(15)   Gosepath, E. M.; Eckstein, N.; Hamacher, A.; Servan, K.; von Jonquieres, G.;

Lage, H.; Györffy, B.; Royer, H. D.; Kassack, M. U. Acquired cisplatin resistance in the

head-neck cancer cell line Cal27 is associated with decreased DKK1 expression and

can partially be

reversed by overexpression of DKK1. *Int. J. Cancer* 2008, *123*, 2013–2019.

(16)   Chou, T.-C. Drug combination studies and their synergy quantification using the Chou-Talalay method. *Cancer Res.* **2010**, *70*, 440–446.

(17)   Piro, G., Roca, M. S., Bruzzese, F., Carbone, C., Iannelli, F., Leone, A., Volpe, M. G., Budillon, A., Di Gennaro, E. Vorinostat potentiates 5-fluorouracil/cisplatin combination by inhibiting chemotherapy-induced EGFR nuclear translocation and increasing cisplatin uptake. *Mol. Cancer Ther.* **2019**, *18*, 1405-1417.

(18)   Chen, S-H., Chang, J-Y. New insights into mechanisms of cisplatin resistance: from tumor cell to microenvironment. *Int. J. Mol. Sci.* **2019**, *20*, 4136

(19)   Autin, P., Blanquart, C., Fradin, D. Epigenetic drugs for cancer and microRNAs: a focus on histone deacetylase inhibitors. *Cancers*. **2019**, *11*, 1530

(20)   Pchejetski, D., Alfraidi, A., Sacco, K., Alshaker, H., Muhammad, A., Monzon, L. Histone deacetylases as new therapy targets for platinum-resistant epithelial ovarian cancer. *J. Cancer Res Clin. Oncol.* **2016**, *142*, 1659-1671

(21)   Bandolik, J.; Hamacher, A.; Schrenk, C.; Weishaupt, R.; Kassack, M. U. Class I-histone deacetylase (HDAC) inhibition is superior to pan-HDAC inhibition in modulating cisplatin potency in high grade serous ovarian cancer cell lines. *Int. J. Mol. Sci.* 2019, *20*, E3052.

(22)   Stenzel, K.; Hamacher, A.; Hansen, F. K.; Gertzen, C. G. W.; Senger, J.; Marquardt, V.; Marek, L.; Marek, M.; Romier, C.; Remke, M.; Jung, M.; Gohlke, H.;

Kassack, M. U.; Kurz, T. Alkoxyurea-based histone deacetylase inhibitors increase cisplatin potency in chemoresistant cancer cell lines. *J. Med. Chem.* **2017**, *60*, 5334–5348.

(23)   Jakobsen, C. M.; Denmeade, S. R.; Isaacs, J. T.; Gady, A.; Olsen, C. E.; Christensen, S. B. Design, synthesis, and pharmacological evaluation of thapsigargin analogues for targeting apoptosis to prostatic cancer cells. *J. Med. Chem.* **2001**, *44*, 4696–4703.

(24)   Grosse, S.; Pillard, C.; Himbert, F.; Massip, S.; Léger, J. M.; Jarry, C.; Philippe Bernard, P.; Guillaumet, G. Access to imidazo[1,2-*a*]imidazolin-2-ones and functionalization through Suzuki–Miyaura cross-coupling reactions. *Eur. J. Org. Chem.* **2013**, *2013*, 4146 – 4155.

(25)   West, C. W.; Estiarte, M. A.; Rich, D. H. New methods for side-chain protection of cysteine. *Org. Lett.* **2001**, *3*, 1205 – 1208.

(26)   Reynolds, D.; Hao, M.-H.; Wang, J.; Prajapati, S.; Satoh, T.; Selvaraj, A*.* Pyrimidine FGFR4 Inhibitors. International Patent WO2015/57938 A1 April 23, 2015.

(27) Dallavalle, S.; Cincinelli, R.; Nannei, R.; Merlini, L.; Morini, G.; Penco, S.; Pisano,

C.; Vesci, L.; Barbarino, M.; Zuco, V.; De Cesare, M.; Zunino, F. Design, synthesis,

and evaluation of biphenyl-4-yl-acrylohydroxamic acid derivatives as histone

deacetylase (HDAC) inhibitors. *Eur. J. Med. Chem.* **2009**, *44*, 1900 – 1912.

(28) Rusche, James R. Compositions including 6-Aminohexanoic Acid Derivatives as

HDAC Inhibitors. U.S. Patent 9,265,734 April 19, 2012.

(29) Mazitschek, R.; Ghosh, B.; Hendricks, J. A.; Reis, S.; Haggarty, S. J.

Photoswitchable HDAC Inhibitors. International Patent WO 2014/160221 A1 October

2, 2014.

(30) Gediya, L. K.; Chopra, P.; Purushottamachar, P.; Maheshwari, N.; Njar, V. C. O. A

new simple and high-yield synthesis of suberoylanilide hydroxamic acid and its

inhibitory effect alone or in combination with retinoids on proliferation of human

prostate cancer cells. *J. Med. Chem.* **2005**, *48*, 5047–5051.

(31) Eckstein, N.; Servan, K.; Girard, L.; Cai, D.; von Jonquieres, G.; Jaehde, U.;

Kassack, M. U.; Gazdar, A. F.; Minna, J. D.; Royer H. D. Epidermal growth factor

receptor pathway analysis identifies amphiregulin as a key factor for cisplatin

resistance of human breast cancer cells. *J. Biol. Chem.* **2008**, *283*, 739–750.

(32)   Marek, L.; Hamacher, A.; Hansen, F. K.; Kuna, K.; Gohlke, H.; Kassack, M. U.;

Kurz, T. Histone deacetylase (HDAC) inhibitors with a novel connecting unit linker

region reveal a selectivity profile for HDAC4 and HDAC5 with improved activity

against chemoresistant cancer cells. *J. Med. Chem.* **2013**, *56*, 427–436.

(33)   Engelke L. H.; Hamacher A.; Proksch P.; Kassack M. U. Ellagic acid and

resveratrol prevent the development of cisplatin resistance in the epithelial ovarian

cancer cell line A2780. *J. Cancer.* **2016**, *7*, 353–363.

(34)   Ciossek, T.; Julius, H.; Wieland, H.; Maier, T.; Beckers, T. A homogeneous cellular

histone deacetylase assay suitable for compound profiling and robotic screening.

Anal. Biochem. **2008**, *372*, 72–81.

(35)   Bonfils, C.; Kalita, A.; Dubay, M.; Siu, L. L.; Carducci, M. A.; Reid, G.; Martell, R.

E.; Besterman J. M.; Li, Z. Evaluation of the pharmacodynamic effects of MGCD0103

from preclinical models to human using a novel HDAC enzyme assay. *Clin. Cancer*

Res. **2008**, *14*, 3441–3449.

(36)   Hoffmann, K; Brosch, G; Loidl, P.; Jung, M. A Non-isotopic assay for histone deacetylase activity. *Nucl. Acids Res.* **1999,** *27, 2057–2058.*

(37)   Schneider, C. A.; Rasband, W. S.; Eliceiri, K. W. NIH image to ImageJ: 25 years of image analysis. *Nat. Methods* **2012**, *9*, 671–675.

(38)   Heltweg, B.; Dequiedt, F.; Verdin, E.; Jung, M. Nonisotopic substrate for assaying both human zinc and NAD+-dependent histone deacetylases. *Anal. Biochem.* **2003**, *319*, 42–48.

(39)   Millard, C. J.; Watson, P. J.; Celardo, I.; Gordiyenko, Y.; Cowley, S. M.; Robinson, C. V.; Fairall, L.; Schwabe, J. W. Class I HDACs share a common mechanism of regulation by inositol phosphates. *Mol Cell.* **2013**, *51*, 57–67.

(40)   Lauffer, B. E. L.; Mintzer, R.; Fong, R.; Mukund, S.; Tam, C.; Zilberleyb, I.; Flicke, B.; Ritscher, A.; Fedorowicz, G.; Vallero, R.; Ortwine, D. F.; Gunzner, J.; Modrusan, Z.; Neumann, L.; Koth, C. M.; Lupardus, P. J.; Kaminker, J. S.; Heise, C. E.; Steiner, P.; Histone deacetylase (HDAC) inhibitor kinetic rate constants correlate with cellular histone acetylation but not transcription and cell viability. *J. Biol. Chem.* **2013**, *288*, 26926–26943.

(41)   Watson, P. J.; Fairall, L.; Santos, G. M.; Schwabe, J. W. Structure of HDAC3 bound to co-repressor and inositol tetraphosphate. *Nature* **2012**, *481*, 335–340.

(42)   Hai, Y.; Christianson, D. W. Histone deacetylase 6 structure and molecular basis of catalysis and inhibition. *Nat. Chem. Biol.* **2016**, *12*, 741–747.

(43)   Gerber, P. R.; Müller, K. MAB, a generally applicable molecular force field for structure modelling in medicinal chemistry. *J. Comput.- Aided Mol. Des.* **1995**, *9*, 251−268.

(44)   Goodsell, D. S.; Morris, G. M.; Olson, A. J. Automated docking of flexible ligands: application of Autodock. *J. Mol. Recognit.* **1996**, *9*, 1−5.

(45)   Gohlke, H.; Hendlich, M.; Klebe, G. Knowledge-based scoring function to predict protein-ligand interactions. *J. Mol. Biol.* **2000**, *295*, 337−356.

(46)   Dittrich, J.; Schmidt, D.; Pfleger, C.; Gohlke, H. Converging a knowledge-based scoring function: DrugScore[2018]. *J. Chem. Inf. Model.* **2019**, *59*, 509–521.

(47)   Sotriffer, C. A.; Gohlke, H.; Klebe, G. Docking into knowledge-based potential fields: a comparative evaluation of DrugScore. *J. Med. Chem.* **2002**, *45*, 1967−1970.

(48)   Baell, J. B.; Holloway, G. A. New substructure filters for removal of pan assay interference compounds (PAINS) from screening libraries and for their exclusion in bioassays. *J. Med. Chem.* **2010**, *53*, 2719−2740.

Insert Table of Contents Graphic and Synopsis Here